

Available online at www.sciencedirect.com**ScienceDirect**Journal homepage: www.elsevier.com/locate/cortex**Research Report****Four new cytoarchitectonic areas surrounding the primary and early auditory cortex in human brains**

Daniel Zachlod ^{a,*}, Britta Rüttgers ^b, Sebastian Bludau ^a,
Hartmut Mohlberg ^a, Robert Langner ^{c,d}, Karl Zilles ^{a,e} and
Katrin Amunts ^{a,b,e}

^a Institute of Neuroscience and Medicine (INM-1), Research Centre Jülich, Jülich, Germany^b C. & O. Vogt Institute for Brain Research, University Hospital Düsseldorf, Heinrich-Heine University Düsseldorf, Düsseldorf, Germany^c Institute of Systems Neuroscience, Medical Faculty, Heinrich Heine University Düsseldorf, Düsseldorf, Germany^d Institute of Neuroscience and Medicine (INM-7), Research Centre Jülich, Jülich, Germany^e JARA-BRAIN, Jülich-Aachen Research Alliance, Jülich, Germany**ARTICLE INFO****Article history:**

Received 14 May 2019

Reviewed 2 August 2019

Revised 15 October 2019

Accepted 21 February 2020

Action editor Stephanie Forkel

Published online 14 March 2020

Keywords:

Cytoarchitecture

Superior temporal sulcus

Brain mapping

Temporal lobe

Insular cortex

ABSTRACT

The architectonical organization of putatively higher auditory areas in the human superior temporal gyrus and sulcus is not yet well understood. To provide a coherent map of this part of the brain, which is involved in language and other functions, we examined the cytoarchitecture and cortical parcellation of this region in histological sections of ten human postmortem brains using an observer-independent mapping approach. Two new areas were identified in the temporo-insular region (areas TeI, TI). TeI is medially adjacent to the primary auditory cortex (area Te1). TI is located between TeI and the insular cortex. Laterally adjacent to previously mapped areas Te2 and Te3, two new areas (STS1, STS2) were identified in the superior temporal sulcus. All four areas were mapped over their whole extent in serial, cell-body stained sections, and their cytoarchitecture was analyzed using quantitative image analysis and multivariate statistics. Interestingly, area TeI, which is located between area Te1 and area TI at the transition to the insula, was more similar in cytoarchitecture to lateral area Te2.1 than to the directly adjacent areas TI and Te1. Such structural similarity of areas medially and laterally to Te1 would be in line with the core – belt – parabelt concept in macaques. The cytoarchitectonic probabilistic maps of all areas show the localization of the areas and their interindividual variability. The new maps are publicly available and provide a basis to further explore structural–functional relationship of the language network in the temporal cortex.

© 2020 The Author(s). Published by Elsevier Ltd. This is an open access article under the CC BY license (<http://creativecommons.org/licenses/by/4.0/>).

* Corresponding author. Institute of Neuroscience and Medicine (INM-1), Research Centre Jülich, Jülich, Germany.

E-mail address: d.zachlod@fz-juelich.de (D. Zachlod).

1. Introduction

Understanding the anatomical foundations of language processing requires disentangling the cortical areas forming the language network. The language network includes, among others, aspects of the superior temporal gyrus and sulcus, located medially and laterally to the primary auditory cortex (Friederici, 2012). At the same time, this region has also been attributed to other functions such as Theory of Mind for the superior temporal sulcus (STS, reviewed in (Hein & Knight, 2008)). To contribute to a better understanding of the role of STS areas in these functions, we investigated the areal segregation and cytoarchitecture of this region in more detail, and computed probabilistic maps in stereotaxic space. While detailed maps for the anterior part including Broca's region have been provided during the last years (Amunts, Schleicher, Burgel, Mohlberg, Uylings et al., 1999; Amunts, Weiss, Mohlberg, Pieperhoff, Eickhoff et al., 2004), there is only sparse knowledge on the cortical segregation of the posterior language region, which may correspond to parts of Wernicke's region (Lichtheim, 1884; Wernicke, 1874). Wernicke's region has been conceptualized as a sensory speech region caudal to the primary auditory cortex at the posterior part of BA22 (see Fig. 1) and parts of the supramarginal gyrus (BA40) in the left hemisphere.

Wernicke's and Lichtheim's original publications were anatomically not explicit, and the location of Wernicke's region was later controversially debated among scientists (Bogen & Bogen, 1976). A recent meta-analysis of neuroimaging findings (DeWitt & Rauschecker, 2012) reported activations linked to speech processing in the mid-to-anterior part of the superior temporal gyrus (STG), located laterally to the primary auditory cortex on Heschl's gyrus. This result questions the location of Wernicke's region in the posterior STG as the functional 'center of speech comprehension' (Binder, 2015, 2017).

Language impairment has been described for different neurological diseases affecting Wernicke's region. It was originally defined in aphasic patients with lesions disturbing semantic speech processing (Wernicke, 1874), but aphasia is not limited to the posterior part of the STG. Lesions within the whole STG can cause aphasia with different clinical symptoms (Mesulam, Rogalski, Wieneke, Hurley, Geula et al., 2014). For schizophrenia, language deficits (Covington, He, Brown, Naçi, McClain et al., 2005) and acoustic hallucinations (Diederken, Daalman, de Weijer, Neggers, van Gastel et al., 2012) are reported, as well as a gray matter loss in the STG (Matsumoto, Simmons, Williams, Hadjulis, Pipe et al., 2001). Autistic patients may also suffer from language deficits (Eigsti, de Marchena, Schuh, Kelley, 2011) and show a hypoperfusion of the left STG (Gendry Meresse, Zilbovicius, Boddaert, Robel, Philippe et al., 2005).

Despite the clinical relevance and the various functions for communication, little is known about the underlying microstructure and cytoarchitectonic parcellation of the temporo-insular and the STS region in the human brain. In former mapping studies (Fig. 1), e.g., by Brodmann (Brodmann, 1909), the STS separates BA22 on the superior temporal gyrus (STG) from BA21 on the middle temporal gyrus (MTG). However,

Brodmann did not show details of the parcellation within the sulcus, and his map does not indicate the precise course of the border between BA22 and BA21.

The parcellation proposed by Von Economo and Koskinas (1925) divided the brain into 107 areas, which are more than twice as many as Brodmann's areas. They identified an area TA on the STG and an area TE1 on the MTG with a common border in the fundus of the STS. Von Economo and Koskinas did not find separable areas in the STS, in contrast to later observations by Hopf (1954), who provided a detailed map of the temporal areas according to myeloarchitectonic criteria and identified an additional area profunda (pf) in the STS.

The temporo-insular region in Brodmann's map (1909) is equivalent to area BA52 (see Fig. 1). It begins anteriorly with the Limen insulae and ends caudally with the Margo insularis posterior. The lateral border is BA41, the medial border is the granular cortex of the Regio insularis. von Economo and Horn (1930) described the region between the insular (JBT) and primary auditory cortex (TC) as the dorsal part of the temporal pole (TG2). This latter area was subdivided into two subareas TG2 α (lateral) and TG2 β (medial). It represents a triangular shaped area with its broadest part towards the temporal pole. Myeloarchitectonically, this region might be part of the Regio temporalis para-insularis, which Hopf (1954) further divided into 3 subareas and the R. temporalis separans medialis with its two subareas.

Galaburda and Sanides (1980) investigated the human auditory cortex on cell-body stained brain sections and identified an area ProA between the insula and the auditory core areas Kam, Kalt. ProA has features of the insular and temporal cortices and is therefore the equivalent area of the temporo-insular region described here. This region was also analyzed on different histochemically stained sections in two studies (Rivier & Clarke, 1997; Wallace, Johnston, Palmer, 2002), which found two areas, AA and MA, on the Planum polare, with area AA being more rostro-lateral than area MA.

The areas identified by different investigators (listed in Table 1) overlap only partially (reviewed for the human auditory cortex in (Moerel, De Martino, Formisano, 2014)). Their exact position and correspondences cannot be directly compared and related to each other. This is partly due to the difficulties in depicting the sulcal surface on a 2D drawing, while a common spatial reference space would provide a framework to superimpose the different findings. A three-dimensional map of the STS might be also compared with findings from functional or structural imaging studies to study the relationship between behavior, brain function and the underlying microscopical anatomy. The aim of our study was therefore to provide a 3D map of the areas on the STG, relying on the same approach as in our previous studies on primary and secondary auditory cortex (Morosan, Rademacher, Schleicher, Amunts, Schormann et al., 2001; Morosan, Schleicher, Amunts, Zilles, 2005). This approach is based on quantitative image analysis and statistical criteria for defining borders between areas in serial, cell-body stained sections of ten human post mortem brains. The areas were reconstructed and registered to a common 3D reference space, where the topography and intersubject variability of the areas can be depicted for each voxel, enabling a direct comparison with in vivo neuroimaging studies. We capitalized on this possibility by using the new maps as spatial masks to query the BrainMap database of neuroimaging studies (www.brainmap.org).

Localisation on historical maps

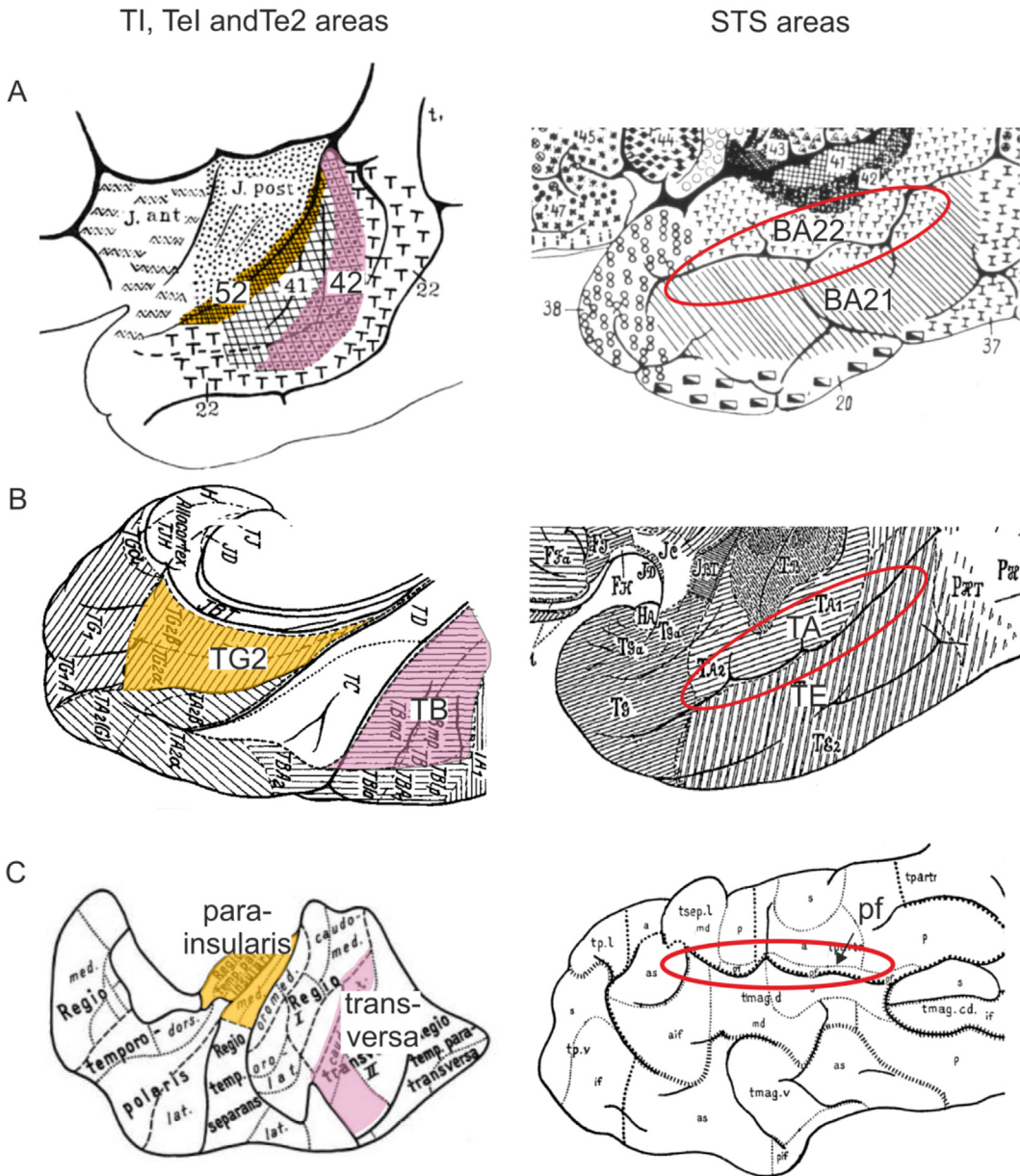


Fig. 1 – Cytoarchitectonic maps of Brodmann (A), von Economo (B) and myeloarchitectonic map of Hopf (C). The areas of temporo-insular region are marked in yellow and the corresponding areas of the Planum temporale in pink. The approximate position of the areas in the superior temporal sulcus (STS) is highlighted by red ellipsoids. The names of the equivalent areas in the classical maps are listed in Table 1.

brainmap.org) to identify experiments reporting activations in any of the newly defined subregions. Analyzing the meta-data associated with each study identified in BrainMap enabled us to objectively and quantitatively characterize the functional roles of the new areas.

2. Materials and methods

2.1. Histological processing of the post mortem brains

Ten brains (5 female, 5 male, 37–85 years old) from the body donor program of the Anatomical Institute at the University of

Düsseldorf were used for cytoarchitectonic analysis (see Table 2). Donors gave their written informed consent, according to the requirements of the Ethics Committee of the University of Düsseldorf. The subjects did not have any neurological disease, except case pm9, who suffered from transitory motor deficits. Handedness was not known. The post mortem delay did not exceed 24 h. After removal from the skull brains were immersed with 4% formalin or in Bodian's fixative for at least 6 months, embedded in paraffin (protocols in the supplement) and completely serially cut into 20 µm coronal sections (Polycut E, Reichert-Jung, Germany). Every 15th section was mounted on gelatin-covered glass slides and silver-stained for cell bodies (Merker B 1983; procedure described in the

Table 1 – Comparison of temporal cortical areas with classical maps.

	Brodmann ^a	von Economo and Koskinas ^b	Hopf ^d	Rivier and Clarke ^e , Wallace ^f	Galaburda and Sanides ^g
TI	52	TG2 ^c	tsep.m/tpari	AA,MA	ProA
TeI					
Te1	41	TC/TD	ttr1	A1, LP	Kam, Kalt
Te2.1	42	TB	ttr2	LA/PA	PaAi, PaAe, Pac, TPt
Te2.2					
Te3	22	TA	tsep.l/tpartr	STA	PaAe,Tpt
STS1			pf		
STS2	21	TE1	tmag.d		

^a Brodmann (1909).^b Von Economo & Koskinas (1925).^c Hopf (1954).^d von Economo & Horn (1930).^e Rivier & Clarke (1997).^f Wallace et al. (2002).^g Galaburda & Sanides (1980).**Table 2 – Brains used for cytoarchitectonic mapping.**

Brain code	Gender	Age [years]	Cause of death	Fresh brain weight [g]
BC01	Female	79	Carcinoma of the bladder	1350
BC03	Male	69	Vascular disease	1360
BC04	Male	75	Acute glomerulonephritis	1349
BC05	Female	59	Cardiorespiratory insufficiency	1142
BC06	Male	54	Cardiac infarction	1622
BC07	Male	37	Cardiac arrest	1437
BC08	Female	72	Renal arrest	1216
BC09	Female	79	Cardiorespiratory insufficiency	1110
BC10	Female	85	Mesenteric infarction	1046
BC13	Male	39	Drowning	1234
BC20	Male	65	Cardiorespiratory insufficiency	1392

supplement). Delineation of areas was performed on every 60th section.

2.2. Observer-independent detection of borders based on the Grey Level Index and analysis of volume

The borders were identified in images of histological sections using statistical criteria and image analysis (Schleicher, Morosan, Amunts, Zilles, 2009; Schleicher, Palomero-Gallagher, Morosan, Eickhoff, Kowalski et al., 2005). For this purpose, rectangular regions of interests (ROIs) on histological sections were digitized (1.01 $\mu\text{m}/\text{pixel}$) with a CCD camera (AxioCamMRm, Zeiss, mounted on a light microscope Axioplan 2 imaging, Zeiss). ROIs were transferred into Grey Level Index (GLI) images using in-house MatLab code. The digitized image was filtered (Gauss filter 1 pixel and 40 pixel), the two resulting images were subtracted to detect the edges of the cell bodies and the ROI was transferred to a binary image. This binary image was superimposed by a $16 \times 16 \mu\text{m}$ grid (see Bludau et al., 2014). Cells cover different fractions of this grid, therefore the Grey Level Index (GLI) was calculated as a measure of the volume fraction of cell bodies in these images (Wree, Schleicher, Zilles, 1982). The outer contour line (border between layers I and II) and the inner contour line at the white matter border were defined. Between these contour lines curvilinear traverses were calculated (Fig. 2C). GLI profiles

were extracted by plotting the GLI values against the cortical depth as abscissa. Since the cortex differs in thickness, between brain regions and brains, the profiles were normalized to a standard length (100%), and divided into 10 equidistant bins. GLI profiles reflect the laminar organization of the cortex, and were used to quantitatively characterize different areas and identify borders between them. Each profile was then described by a ten-element feature vector containing the mean GLI value, kurtosis, standard deviation and skewness, as well as the first derivatives of the same elements. The multivariate distance between feature vectors of neighboring sets of profiles (block size range from 12 to 24 profiles) was described by the Mahalanobis distance (MD, Fig. 2A) function (Mahalanobis, Majumdar, Yeatts, Rao, 1949). MD as a measure of the dissimilarity of neighboring blocks of profiles was computed at every profile position using a sliding window procedure. Maxima in the MD function represent changes in the laminar organization of the cortex, thus indicating a putative position of a border. Maxima were accepted as relevant borders, when they were found for at least two block sizes (Fig. 2B) and in three neighboring sections at the same position.

The identified areas were labeled over their whole extent in the high-resolution scans of sections (1200 dpi), and volumes of the areas were calculated based on stereological principles in each hemisphere and brain, and the volumes were

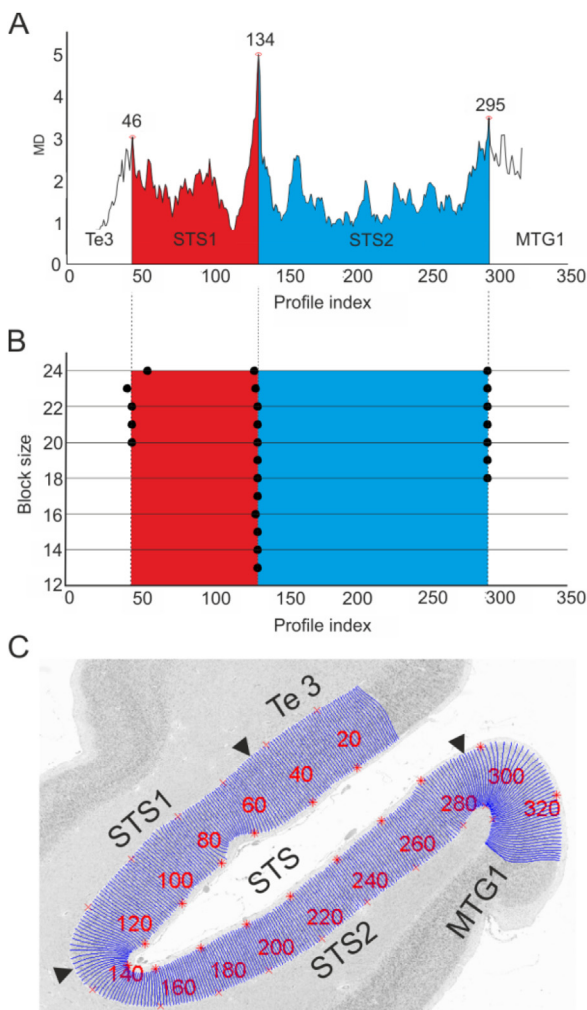


Fig. 2 – Observer-independent detection of borders on cell-stained micrographs. A) The Mahalanobis distance (MD) is plotted against the profile index. MD shows significant maxima at profile positions 46, 134 and 295 indicating the borders of STS1 and STS2. B) The position of the borders was tested for different block sizes ($n = 12\text{--}24$). C) ROI with traverses in blue, along which GLI profiles were calculated as estimates of changes in cytoarchitecture from the layer I/layer II border to the cortex/white matter border. The borders of the areas are marked with black arrow heads at the profile number where the MD function has a maximum and the areas are labeled.

corrected for the shrinkage (Amunts, Armstrong, Malikovic, Hömke, Mohlberg et al., 2007; Amunts, Kedo, Kindler, Pieperhoff, Mohlberg et al., 2005). Shrinkage factors were calculated as the ratio between the fresh volume and the volume after fixation, whereas the fresh volume was estimated from the fresh brain weight and the brain density of 1.033 g/mm³ mentioned in Kretschmann (1971).

$$V = s \cdot T \cdot x \cdot y \cdot \sum A_i \cdot F$$

$$V = \text{areal volume } [\text{mm}^3]$$

$$s = \text{section between scans}$$

T = section thickness (20 µm).

x, y = length and width of the pixel (21.2 µm).

A_i = areal surface in all measured sections (in pixel).

F = shrinkage factor.

Calculated areal volumes were related to the brain volume before embedding and the following histological procedures. These volume fractions of the areas were tested for volume differences in gender and hemispheres with a pair-wise permutation test (Bludau, Eickhoff, Mohlberg, Caspers, Laird et al., 2014; Eickhoff, Paus, Caspers, Grosbras, Evans et al., 2007).

2.3. Discriminant analysis of mean areal GLI profiles

Three ROIs were manually selected per hemisphere and area showing an almost horizontally layered cortex. The three ROIs were distributed over the whole extent of the area to ensure that cortical microstructure is representative of the area. Based on these three ROIs, mean GLI profiles of 45 profiles (15 profiles in each ROI) were calculated. Mean feature vectors were generated for each area based on these mean GLI profiles. Based on these feature vectors a discriminant analysis was calculated using the Euclidian distance and the Ward linking procedures (Ward, 1963). The results were visualized in a dot plot and differences in the GLI-profiles, i.e., the laminar pattern of the areas, are shown by confidence ellipses of the sample means ($p > .95$).

2.4. 3D-reconstruction of areas and stereotaxic maps

Histological sections of each postmortem brain were 3D reconstructed. Therefore, the scans of the sections were registered to the magnetic resonance imaging (MRI) dataset and blockface images taken prior to histological processing with in-house software using linear and non-linear transformations to correct for deformations during histological techniques. By applying the same transformation parameters as used for the 3D reconstruction of the whole post mortem brains, the delineated areas were 3D reconstructed and then registered to the reference space of the T1 weighted, single-subject template of the Montreal Neurological Institute (MNI) (Collins, Neelin, Peters, Evans, 1994; Evans, Collins, Mills, Brown, Kelly et al., 1993; Holmes, Hoge, Collins, Woods, Toga et al., 1998) by using affine transformations and nonlinear elastic registration (Hömke, 2006). They were registered to the anatomical reference space, which is adjusted to the anterior commissure as origin of the coordinate system (Amunts et al., 2005). Probability maps (pmaps) of the analyzed areas from different individual brains were then calculated, which indicate in how many brains an area is found in a certain voxel. They reflect the intersubject variability in localization and extent of the areas. Finally, using the same method, the areas were also transferred to the average MNI (ICBM 152 casym) and the so-called BigBrain template (Amunts, Lepage, Borgeat, Mohlberg, Dickscheid et al., 2013) to offer mapping results in different, widely used template spaces.

These maps were then annotated and integrated to the HBP (Human Brain Project) Atlas (<https://www.humanbrainproject.eu/en/explore-the-brain/>) as a publicly available resource and to the JuBrain atlas (<https://jubrain.fz-juelich.de>).

juelich.de/apps/cytoviewer/cytoviewer.php). On the basis of the pmaps, a non-overlapping map, i.e., a Maximum Probability Map (MPM) was calculated for each area (Eickhoff et al., 2007; Eickhoff, Stephan, Mohlberg, Grefkes, Fink et al., 2005). In the MPM, each voxel was assigned to the area with the highest probability.

2.5. Quantitative functional profiling

To assess the functional significance of the cytoarchitectonically delineated brain areas in an objective and quantitative manner, we analyzed the association of these regions with descriptors for cognitive processes as provided by the Brain-Map database (www.brainmap.org (Laird, Eickhoff, Kurth, Fox, Uecker et al., 2009)). This curated database contains the result coordinates from thousands of published task-related neuroimaging studies along with meta-data that describe the paradigm class (i.e., the specific task category) employed by any given experiment according to a pre-specified taxonomy ((Fox, Laird, Fox, Fox, Uecker et al., 2005); see www.brainmap.org/scribe). By filtering the database for experiments reporting activation in a given area of interest and statistically analyzing the psychological descriptor (paradigm class, PC) of the selected experiments, functional roles of individual areas can be objectively characterized. Our analysis was based on 7937 “normal mapping” experiments performed in healthy adults, excluding intervention studies and comparisons between samples from different populations. Numbers of studies included in the analysis for each cytoarchitectonic area are listed in *Supplementary Table S1*.

We analyzed the functional descriptors of BrainMap experiments associated with each of our areas of interest by way of forward and reverse inference. Forward inference tested whether the probability of finding activation in the area of interest given a particular paradigm class [$P(\text{Activation} | \text{PC})$] was higher than the baseline probability of finding activation in that area across the entire database [$P(\text{Activation})$]. Binomial tests were employed to assess significance at $p < .05$, corrected for multiple comparisons by controlling the false-discovery rate (FDR). Reverse inference identified the most likely PCs given activation in the area of interest. This likelihood [$P(\text{PC} | \text{Activation})$] was derived from $P(\text{Activation} | \text{PC})$, $P(\text{PC})$ and $P(\text{Activation})$ according to Bayes’ rule. Its significance was assessed by chi-square tests ($p < .05$, FDR-corrected for multiple comparisons).

The specificity and commonalities of the functional profiles of a given pair of areas (e.g., left vs right homotopic regions) were examined via contrast and conjunction analyses, respectively. These analyses were restricted to those experiments in BrainMap that activated either area of a given pair, making them somewhat less conservative than the tests for main effects against the entire database, as described above. For differential forward inference, we compared the activation probabilities between two areas given a particular PC; for differential reverse inference, we compared the probabilities of a particular PC being employed given activation in one versus the other area of a given pair (Eickhoff, Bzdok, Laird, Roski, Caspers et al., 2011; Langner, Cieslik, Behrwild, Roski, Caspers et al., 2015). The results of these quantitative comparisons were thresholded at $p < .05$ (FDR-corrected for

multiple comparisons). For both forward and reverse inference, conjunction analyses using the strict minimum t-statistic identified significant intersections of PCs between the two areas of a given pair thresholded at $p < .05$ (Bonferroni-corrected for multiple comparisons).

2.6. Surface-based representation of the areas in the BigBrain

The new areas were additionally mapped in the BigBrain (Amunts et al., 2013), which was the eleventh brain, using the same mapping approach as for the brains forming the data basis of the pmaps. The mapping of the areas in the BigBrain (Table 2, BC20) resulted in a 3D representation with high in-plane and out-of-plane resolution (distance between sections up to 300 μm). This is important in particular for the small and geometrically complex areas such as TI. Maps of the areas were reconstructed in 3D and projected on surfaces models of the BigBrain data set (publicly available at the website <https://bigbrain.loris.ca>). To ensure that the areal surface is not over- or underestimated, which may occur in case of the complex geometry of the sulcal areas, we computed a middle cortical surface from the provided inner and outer surfaces (Fig. 3). The volume labels were projected onto this middle surface and for every cytoarchitectonic area an unambiguous label was assigned to each vertex point of the triangulated surface. The surface area of the cytoarchitectonic areas with label A was calculated by adding up the areas of all triangular areas belonging to a vertex label A multiplied by one third. Volumes of brain areas were calculated by multiplying the areal surface by the mean cortical thickness of the area A_i . In addition, the exact geometric volume defined by the polyhedron volume enclosed between the inner and outer surface was calculated for a comparison with the mean areal volumes and to decide whether the mean areal surface is a good approximation for the areal extent. The difference between the middle volume and the geometrical volume was less than 4%.

2.7. Cytoarchitectonic analysis of neighboring, previously mapped areas

Previously mapped areas Te2.1 and Te2.2 (Clarke & Morosan, 2012; Morosan, Rademacher, Palomero-Gallagher, Zilles, 2005) of the Planum temporale (Figs. 1 and 4) were re-analyzed, to obtain the same set of data as in the present study, and to compare them between each other without a methodical bias. GLI profiles of the previous study were used for cluster- and volumetric analysis. Probability maps and maximum probability maps of areas Te2.1 and Te2.2 were recalculated with present tools to create a consistent and complete map of the (posterior) superior temporal gyrus.

3. Results

Four new areas, TeI and TI in the temporo-insular region and STS1 and STS2 in the mid to anterior STS, were identified. The areas are adjacent to the previously described areas Te1, Te2 and Te3 (Fig. 4). As a result, a complete map covering the superior temporal gyrus was computed.

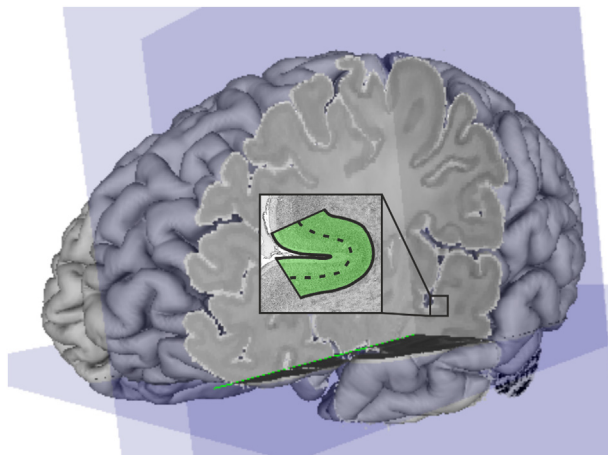


Fig. 3 – Areal delineation in the BigBrain. The areas were additionally mapped in the BigBrain (<https://bigbrain.loris.ca>) by defining an inner and outer contour line for the area (Wagstyl, Lepage, Bludau, Zilles, Fletcher et al., 2018). The temporo-insular area TI (green) is shown in the insert in coronal plane. For the surface-based representation of the areas, the middle surface (dashed line) was calculated.

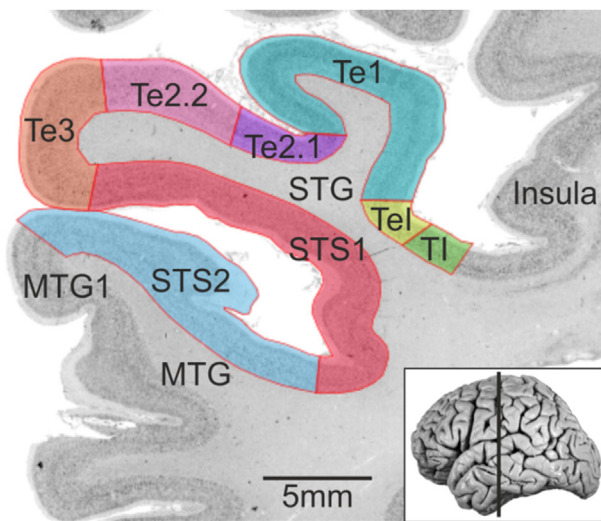


Fig. 4 – Localization of the STG areas on a coronal section. Coronal section of the temporal lobe (position indicated in insert). The areas TI and Tel are medially adjacent to the primary auditory cortex (Te1) close to the insular cortex. The secondary auditory areas Te2.1 and Te2.2 are sulcal areas, and do not reach crown of the superior temporal gyrus (STG), where Te3 starts. STS1 and STS2 are located in the superior temporal sulcus (STS), and occupy its lower and upper bank, respectively. Area MTG1 is a yet uncharted region of the middle temporal gyrus (MTG), laterally adjacent to STS2.

3.1. Cytoarchitecture of areas Tel and TI

The temporo-insular region consists of two distinct areas, Tel and TI. Tel represents the more lateral one, directly adjacent

to the primary auditory cortex (Te1). TI is more medially located, close to the circular sulcus and the insular cortex. Tel has, in comparison to TI, a slightly broader and more densely packed layer II (Fig. 5C). The medium sized cells in layer III are equally distributed in TI with the highest density in layer IIIb as compared to Tel where this maximal density is found in IIIc. Generally, layer III seems to be less dense in TI than in Tel. In Tel the cells of layer III show a columnar like appearance. The other layers show less pronounced differences between these two areas, but are clearly distinct from the primary auditory and insular cortex.

Tel and TI can be distinguished from the primary auditory and insular cortex by a dense layer II and densely packed layers V and VI with small to medium sized cells (Fig. 5B and D). In contrast to Te1, Tel has higher cell densities in layers V and VI (Fig. 5B). Besides, Tel has larger pyramidal cells in layer III which show a more obvious columnar distribution. Layer IV has more granular cells in Te1 than in Tel.

The insular area Id1 (Kurth, Eickhoff, Schleicher, Hoemke, Zilles et al., 2010) can be separated from TI by a less dense layer II which shows no clear-cut border towards layer III (Fig. 5D). The pyramidal cells in layer III are smaller and the cell density increases towards area TI. The granular cells of layer IV are loosely packed in Id1. Layer V has medium sized pyramidal cells in Id1. Layer V and VI are broader in area TI than Id1.

3.2. Cytoarchitecture of areas STS1 and STS2

Area STS1 has a dense layer II with no sharp border towards layer III. Layer IIIc has smaller pyramidal cells compared to area Te3 (Fig. 6D). The granular cells in layer IV are organized in clusters and the layer appears relatively broad. Layer V is less dense than layer VI. Layer VI is clearly visible and has a sharp boundary towards the white matter. Area STS2 has a dense and compact layer II with a sharp border towards layer III (Fig. 6C). Layer III is dominated by medium to large elongated pyramidal cells in IIIc, which covers nearly half of layer III. Layer IV is relatively broad and columnar organized. The cells in layers V and VI are of the same size and distribution so that the border between V and VI is not always clearly visible. The white-matter border is relatively sharp.

Areas STS1 and STS2 can be clearly distinguished from neighboring areas. Dorsal to STS1, there is a long-stretched area on the convexity of the superior temporal gyrus, Te3 (Morosan, Schleicher, et al., 2005; Fig. 6D). It has broad granular layers II and IV. Layer IIIc is prominent. It consists of large and densely packed pyramidal cells. Layer V is rather cell dense. The cells are vertically organized in columns (“organ pipes” by Von Economo & Koskinas, 1925). The inner granular layer is thicker in Te3 than in STS1. Te3 has no sharp cortex/white-matter boundary.

Ventral to areas STS1 and STS2 we identified a yet unmapped area at the middle temporal gyrus (MTG), which we called MTG1 (Fig. 6A). MTG1 is characterized by a less dense layer II, which is broader in MTG1 than in STS2, and has no sharp border to layer III. Layer III a/b has a low cell density. Layer IIIc is thinner than in STS2 without prominent large pyramidal cells at the transition to layer IV. It appears as a

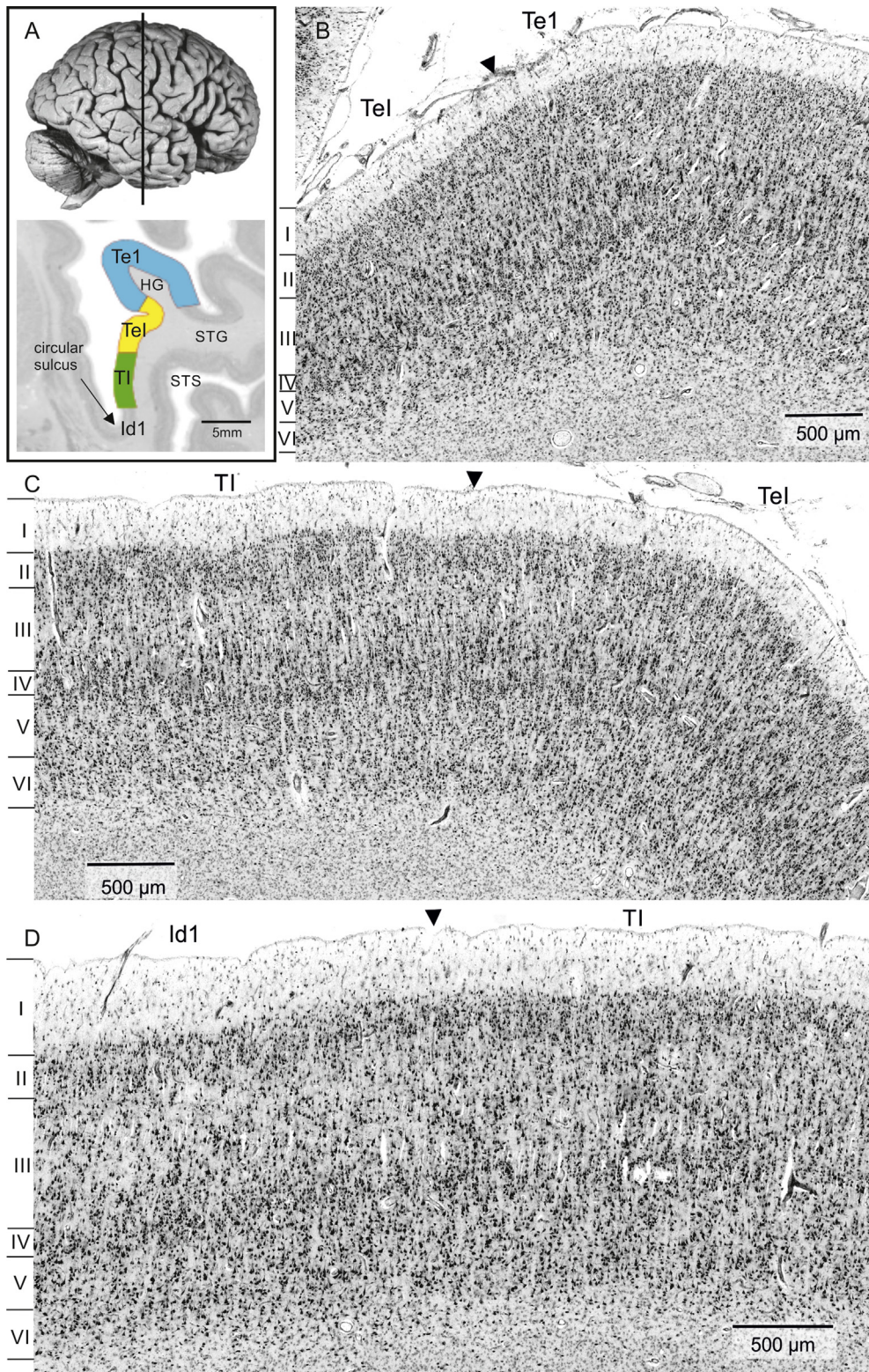


Fig. 5 – Cytoarchitecture and cortical borders (arrow heads) of areas of the Planum polare (A). Areas Tel and neighboring primary auditory area Te1 (B); Tel and TI as well as TI and neighboring dysgranular insular area Id1 (Kurth et al., 2010; D) are shown. Cortical layers are indicated on the left. One main characteristic to distinguish the areas is layer III. Te1 has larger pyramidal cells than Tel (B); Tel has the highest cell density in IIIc, whereas the cells are equally distributed in TI (C) and area Id1 has a cell-sparse layer III (D).

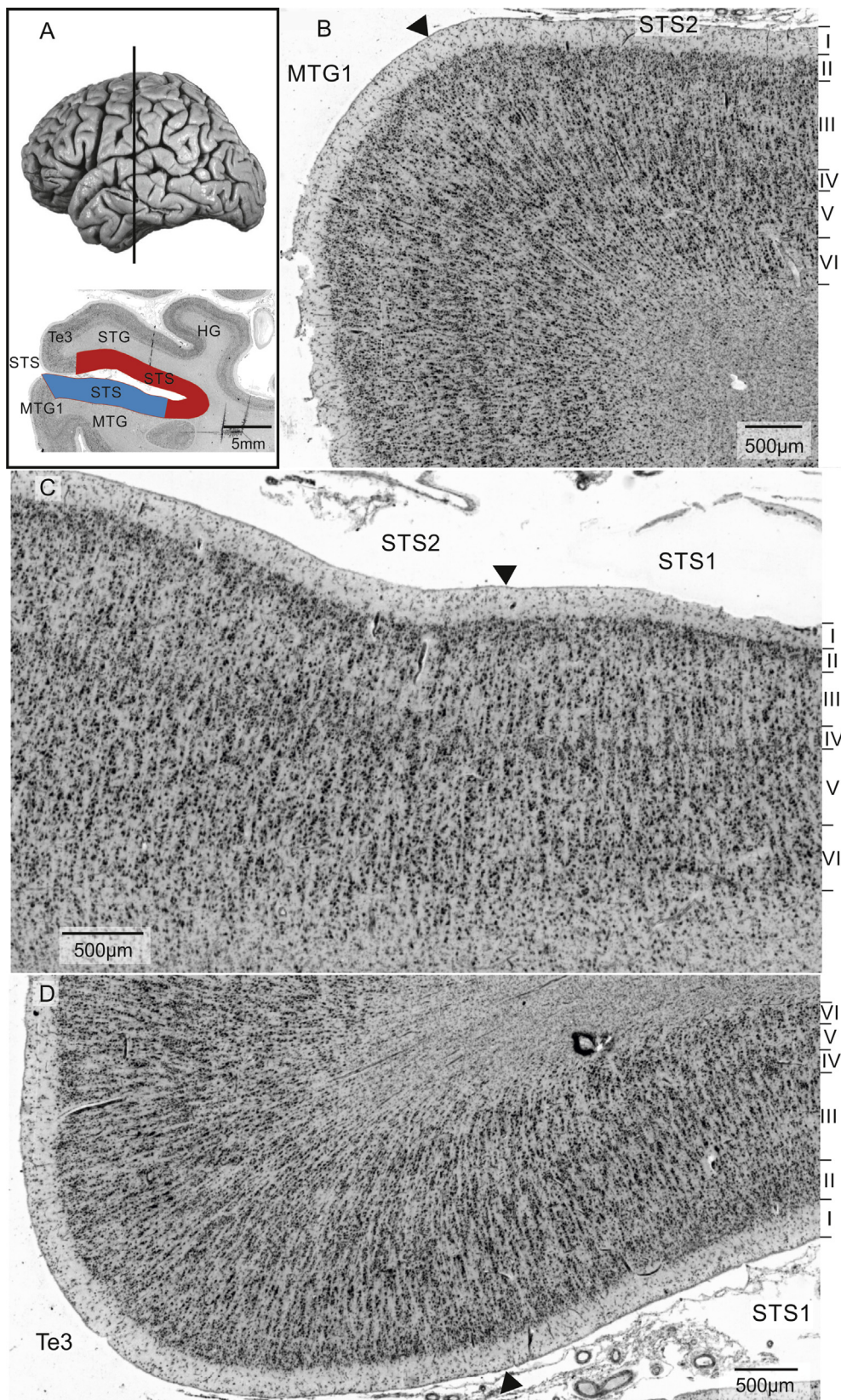


Fig. 6 – Cytoarchitecture and cortical borders (arrow heads) of areas of the STS region (A). Areas STS2 and neighboring area MTG1 (B); STS1 and STS2 as well as STS1 and neighboring area Te3 (Morosan et al., 2005; D) are shown. Cortical layers are indicated on the right. The characteristic feature of MTG1 is the gap between the pyramidal cells in III and layer IV (B). STS2 has a compact and denser layer II than STS1 (C) and Te3 has large pyramidal cells in layer III (D).

light, cell sparse ribbon. Layers III and V have a less prominent columnar organization than STS2. Layer V has larger pyramids in its superficial part, close to layer IV. Towards layer VI, the pyramidal cells become smaller and less cell dense.

3.3. Cytoarchitecture of areas Te2.1 and Te2.2

Based on previous research of our group, we extended the current analysis with data from the secondary auditory areas Te2.1 and Te2.2 (Clarke & Morosan, 2012; Morosan, Rademacher, et al., 2005) and the primary auditory cortex (Morosan et al., 2001), and compared their cytoarchitecture based on image analysis and multivariate statistics (Fig. 7). Areas Te2.1 and Te2.2 are located between the primary auditory cortex, area Te1, and area Te3 on the superior temporal gyrus.

Area Te2.1 has a large and cell sparse layer III and thin, but cell dense layers V and VI. It can be clearly delineated from the koniocortical area Te1 with its prominent layer IV (Fig. 7B). In contrast to Te2.1, area Te2.2 (Fig. 7C) has a broader layer II with a higher cell density and larger pyramidal cells in IIc. At the border to Te3 (Fig. 7D), layer IIc of Te2.2 becomes more prominent with its large pyramidal cells and layer V is more cell dense.

These cytoarchitectonic characteristics are well reflected by the shape of the GLI profiles (Fig. 8). For example, area Te2.1 has a thin layer V which becomes broader in Te2.2.

3.4. Quantification of cytoarchitectonic differences and similarities of auditory areas

The GLI-profiles of eight auditory areas Te1, Te2.1, 2.3, 3, TeI, TI, STS1 and STS2 were subjected to a discriminant analysis in order to identify those areas that have a similar cytoarchitecture or, on the contrary, are most distinct from each other. The results are presented in Fig. 9. It shows the differences in cytoarchitecture between the areas by distances in the plot of the discriminant analysis. Each area is represented by an ellipsoid and a set of 20 dots (2 hemispheres, 10 brains). The variance in the localization of the dots reflects the cytoarchitectonic, intersubject variability. Primary auditory area Te1 is clearly separated from the other areas. Area TI forms a cluster that is also separated from the other ones. It is relatively homogenous, indicating that intersubject variability is low. Area TeI has an intermediate position between TI, located close to the insula, and the other auditory areas, laterally adjacent to TeI. Interestingly, area TeI's cytoarchitectonic features are more similar to those of area Te2.1 and STS1, which are located at some distance, laterally from Te1. TeI is less similar to the direct neighboring areas Te1 and TI. The cytoarchitecture of area Te2.2 is similar to Te3; both areas are different from the STS areas.

3.5. Localization and interindividual variability

The cytoarchitectonic probabilistic maps show the stereotaxic localization and extent of the areas, and quantify their interindividual variability in standard reference space (Fig. 10). The probabilistic maps well represent the localization of the areas in the individual brains, and reflect the relationships of areas with respect to sulcal landmarks.

Intersubject variability differs between the areas, but also with respect to their localization in the brain. The

temporo-insular areas, TeI and TI, are deeply buried in the Sylvian fissure. The areas show a low degree of variance in the analyzed ten brains. TI is the most medial area and reaches more rostrally than TeI. The areas of the Planum temporale showed a higher variability in the left hemisphere (Te2.1 rostral, Te2.2 caudal) as compared to the right. In the right hemisphere only Te2.2 was highly variable in its most rostral part. The sulcal areas STS1 and STS2 never extended on free lateral surface of the superior and middle temporal gyrus. The variability of STS1 is rather similar at the rostral and caudal end, whereas STS2 showed a somewhat lower variability at the rostral than at the caudal end.

The interindividual variability in volumes of the areas (Table 3) varied between the areas with the Te2 areas being more variable than the temporo-insular and STS areas. Left-right and sex differences were not significant ($p > .05$).

3.6. Extent of the areas on the surface of the BigBrain

The temporo-insular and STS areas were additionally mapped in the BigBrain and areas were reconstructed on the surface to calculate the middle areal surface, the middle areal thickness and the areal volume (Table 4). The middle areal surface was depicted on the BigBrain and shown in Fig. 11.

3.7. Neighborhood relationships of areas and localization with respect to anatomical landmarks

Areas TeI and TI cover large parts of the Planum polare, medio-rostrally adjacent to Heschl's gyrus (Fig. 12). The posterior part of TeI can be approximately delineated by the Sulcus temporalis transversus primus. More anteriorly the border is found on the most medial part of Heschl's gyrus. Te1 is the laterally neighboring area of TeI in the posterior part, while more rostrally, TeI borders Te3. There is no landmark for the rostral end. Both areas do not reach the temporal pole, and TI ends more rostrally than TeI. The medial border of TI is always area Id1 of the insular cortex (Kurth et al., 2010), close to the circular sulcus on the STG. TI, however, never crosses the fundus of the circular sulcus.

The Planum temporale contains two areas, Te2.1 and Te2.2. Te2.1 is located laterally to Heschl's gyrus. Its approximate rostral border is formed by Heschl's sulcus. Its caudal end is not limited by a landmark, but is always found in the posterior part of Heschl's gyrus, where it is replaced by Te2.2. This area neighbors Te1 and Te3. Te2.2 is found only in the horizontal part of the Sylvian fissure. The position of STS1 and STS2 in the STS is relatively stable across the coronal sections in all ten brains. Both are separated approximately by the fundus of the STS, and their lateral border is close to the crown of the gyrus. The areas do not cover the lateral part of the gyrus. STS1 is located at the upper bank of the STS, laterally to Heschl's gyrus, while STS2 occupies its lower bank. Caudally both STS areas end approximately at the position where Heschl's gyrus ends. The rostral end is not indicated by a landmark. STS1 does not extend to the Limen insulae, whereas STS2 ends in the middle between the Limen insulae and the temporal pole.

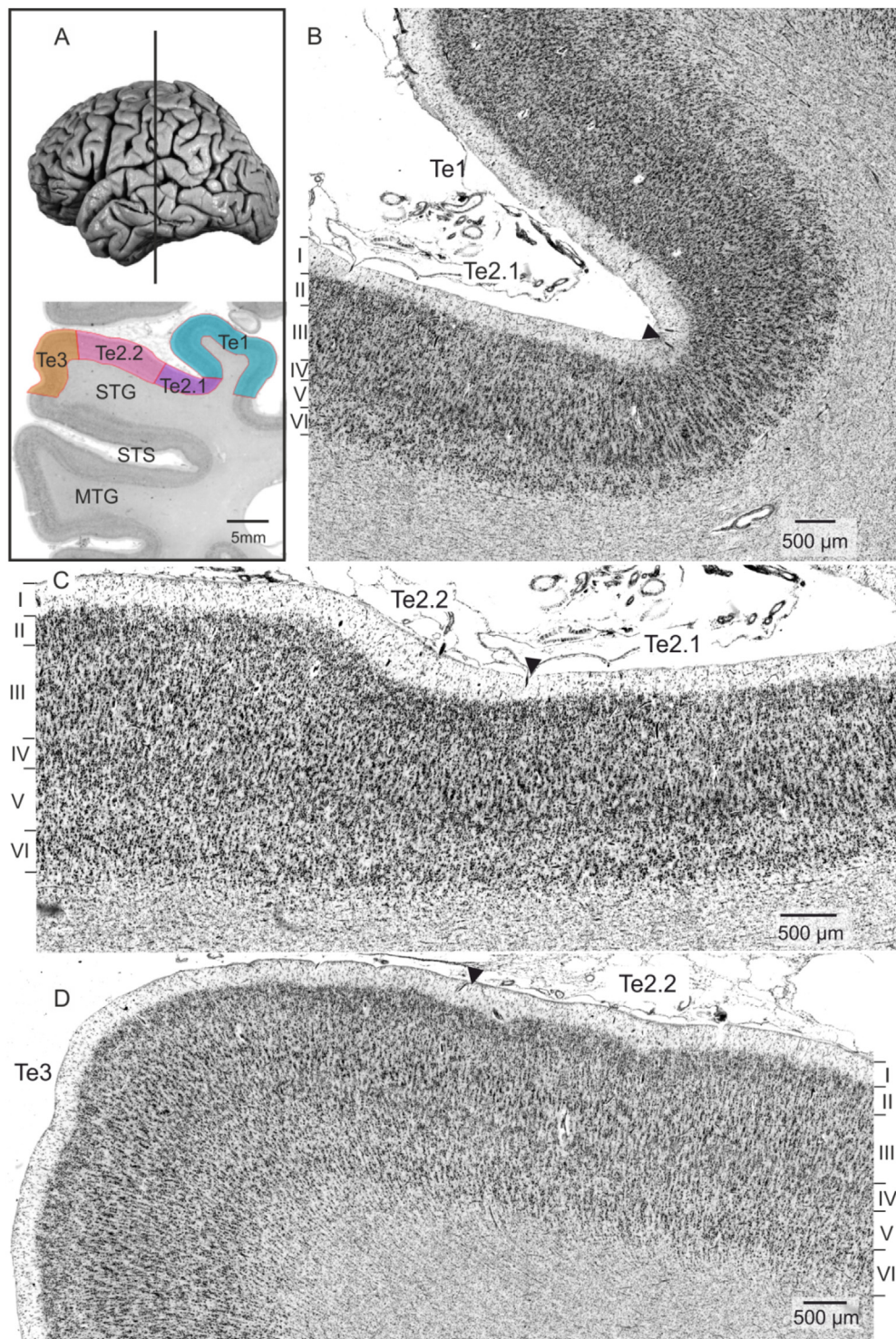


Fig. 7 – Cytoarchitecture and cortical borders (arrow heads) of areas on the Planum temporale (A). Areas Te2.1 and neighboring primary auditory area Te1 (B); Te2.1 and Te2.2 as well as Te2.2 and neighboring area Te3 (Morosan et al., 2005; D) are shown. Cortical layers are indicated in Roman numerals. Te1 is characterized by a prominent layer IV (B); Te2.1 has a rather cell sparse layer III compared to larger cells in IIc in Te2.2 (C); Te3 has large pyramidal cells in IIc (D).

3.8. Functional characterization of the described cytoarchitectonic areas

The maximum probability maps were used to carry out region-specific quantitative functional profiling by querying

the BrainMap database of neuroimaging studies. Paradigm classes associated above chance with activation in a given area of interest were tested via forward [$P(\text{Activation} \mid \text{Paradigm})$] and reverse inference [$P(\text{Paradigm} \mid \text{Activation})$]. Above-chance associations between a given area and a given

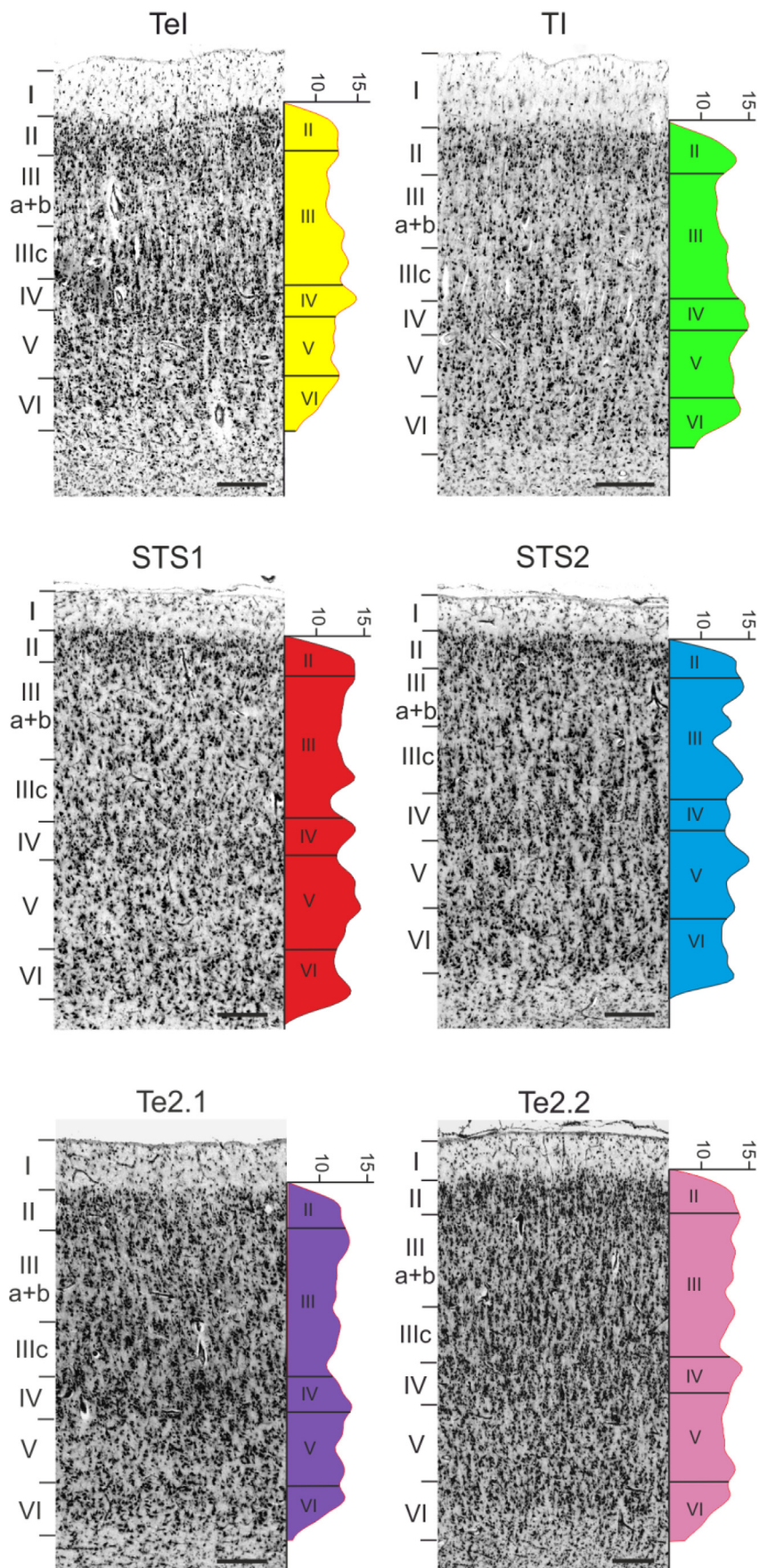


Fig. 8 – Cytoarchitecture and corresponding GLI profiles. The GLI profiles reflect the laminar changes of the volume fraction of cell bodies, i.e., cytoarchitecture. For example, note that the cells in layer III of area TI are equally distributed, whereas there are more and larger cells in layer IIIc in area TeI resulting in a characteristic increase in the GLI-profile. Scale bar 250 μ m.

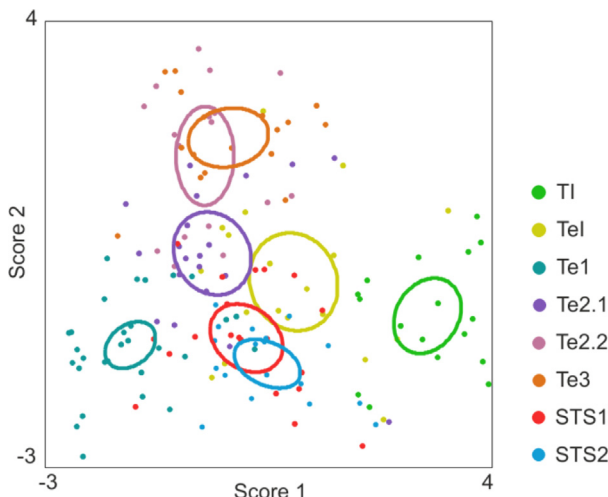


Fig. 9 – Discriminant analysis of GLI profiles. The GLI profiles of all areas of the STG were compared in a discriminant analysis. Each dot represents data from one hemisphere. Colored circles indicate the centroids for each area. The primary auditory cortex (Te1; petrol) can be clearly separated from areas of the higher auditory cortex. The same is true for area TI. In its cytoarchitectonic characteristics, area Tel (yellow) resembles more area Te2.1 (purple) than neighboring area TI (green).

paradigm class according to both types of inference are listed in Table 5.

The TI area of the left hemisphere is activated by music comprehension, drawing and passive listening. In the right hemisphere, it is only activated by pain monitor/discrimination tasks. Beginning from Tel to Te3, the areas were mainly activated by acoustic tasks and showed no obvious lateralization except from passive listening, which was left-lateralized in Te1, Te2.1, and Te2.2 but not in the temporo-insular and STS areas (see Supplementary Fig. S1+S2). The STS areas differ largely between STS1 and STS2. While the left STS1 showed activations related to figurative language and semantic discrimination tasks, the left STS2 is activated by tasks which involved episodic recall, the imagination of scenes and objects, or self-control (delay discounting). These functional differences were separately tested for the new areas in each hemisphere and for lateralization within each area (Supplementary Fig. S3+S4). Lateralization shown in Table 5 was corroborated. Right area TI was activated by pain, whereas its left counterpart was activated by drawing and music comprehension. The area Tel showed no significant difference between the hemispheres. A left-side preference was found in STS1 for drawing and in STS2 for covert reading, delay-discounting and semantic discrimination.

4. Discussion

The present study yielded maps of the superior temporal gyrus/sulcus with four new cytoarchitectonic areas, providing new insights into the cytoarchitectonic organization of an

important part of this language-related region with presumably different functionalities. Advantages of the cytoarchitectonic study are the definition of borders based on quantitative measures, the three-dimensional nature of the maps, the consideration of intersubject variability in localization and cytoarchitecture, as well as the analysis of potential interhemispheric and sex differences. Two of the newly identified areas, Tel and TI, are located medially to the primary auditory cortex, close to the insular cortex. By its cytoarchitecture and localization, TI is a temporo-insular transition area, whereas Tel has more characteristics in common with areas of the temporal lobe. Tel is more similar to area Te2.1 than to TI based on its cytoarchitecture. The other two newly defined areas, STS1 and STS2, located in the superior temporal sulcus, are similar in their microstructure and showed larger differences to primary and higher auditory areas (Te1-3). All areas were delineated based on statistical criteria and image analysis to verify the areal borders and are represented in a standard reference brain showing their interindividual variability and maximum probability.

4.1. Interpretation of TI areas in the context of other maps

The two areas of the temporo-insular cortex, Tel and TI share features with areas in former classical maps. In Brodmann's map (1909), the homolog area seems to be BA52, which was not further subdivided. BA52 ends at the Limen insulae, while our cytoarchitectonic delineation shows that the temporo-insular region reaches more rostrally. The caudal border seems to be comparable. Brodmann described the border to the medial area as granular insular cortex. The present study found that TI has a border with a dysgranular insular region, which was confirmed by former parcellations (Kurth et al., 2010). Von Economo und Horn (1930) divided the temporo-insular region into two areas: the insular-like, medial TG2 β and the lateral area TG2 α , which shares cytoarchitectonic features of other temporal areas. This is in line with the cytoarchitecture and position of Tel and TI, but both areas are ellipsoidal in shape, which is in contrast to the rather triangular shaped region TG2 of von Economo and Horn (1930). The latter, however, was not confirmed by later studies. The anterior end of Economo's TG2 reaches the lateral part of the STG, whereas the new areas TI and Tel are buried in the Sylvian fissure. Nevertheless, TG2 overlaps in large parts with the temporo-insular areas of this study. In comparison of the present maps with the myeloarchitectonic maps of Hopf (1954), we can assume that his areas tpari.im and tpari.l are parts of our new areas. The border between the Regio temporalis parainsularis and separans (Hopf, 1954) are in line with our cytoarchitectonic delineation of TI and Tel. In the temporo-insular delineation of Galaburda and Sanides (1980) ProA was reported to have both insular and temporal characteristics. This is also true for the delineation of the temporo-insular region of this study, which showed a further subdivision into a more insular-like (TI) and a more temporal-like area (Tel). Recent histochemical studies investigating the supratemporal plane found two areas in the temporo-insular region (Rivier & Clarke, 1997; Wallace et al., 2002) called AA and MA, with area AA being located more rostro-laterally than area MA. However, according to our

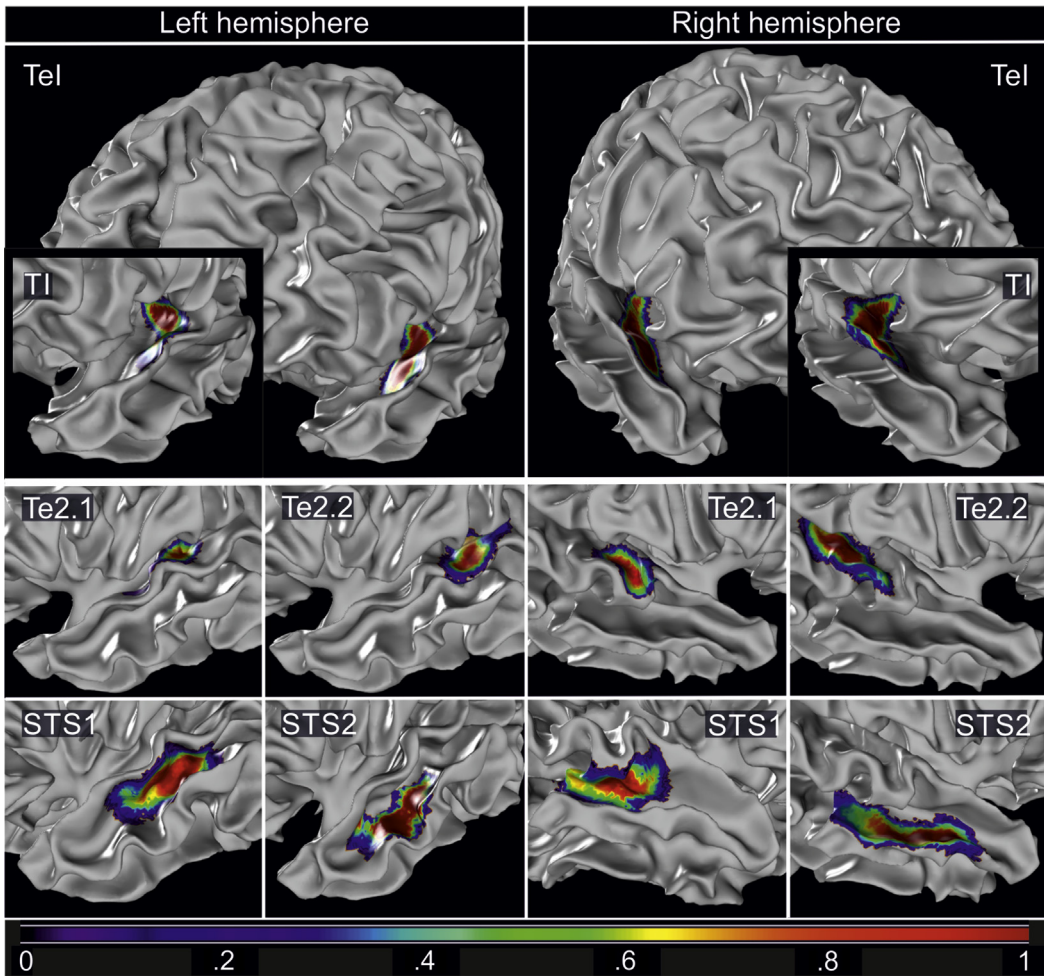


Fig. 10 – Probabilistic maps (pmaps) of the identified areas. The maps indicate color-coded interindividual variability in the stereotaxic MNI Colin 27 template brain. E.g., red regions correspond to a probability of at least 80%. Maps are available at <https://jubrain.humanbrainproject.eu>.

Table 3 – Volumes of the investigated areas. Left right differences were not significant ($p > .05$).

Area	Left hemisphere	Right hemisphere	p-value left vs right	p-value male vs female
TI	572 mm ³ (±202)	610 mm ³ (±123)	.61	.44
TeI	704 mm ³ (±221)	754 mm ³ (±218)	.27	.36
Te2.1	744 mm ³ (±499)	501 mm ³ (±212)	.10	.55
Te2.2	1458 mm ³ (±895)	1407 mm ³ (±523)	.98	.06
STS1	1921 mm ³ (±363)	2094 mm ³ (±598)	.21	.42
STS2	2957 mm ³ (±643)	3135 mm ³ (±574)	.36	.65

Table 4 – Mean surface of the areas in the BigBrain.

area	middle surface [mm ²]	middle thickness [mm]	middle volume [mm ³]
TI right	380	2.4	902
TI left	402	2.3	906
TeI right	241	2.6	625
TeI left	428	2.5	1085
STS1 right	1164	2.7	3110
STS1 left	903	2.7	2458
STS2 right	1377	2.6	3600
STS2 left	1156	2.7	3147

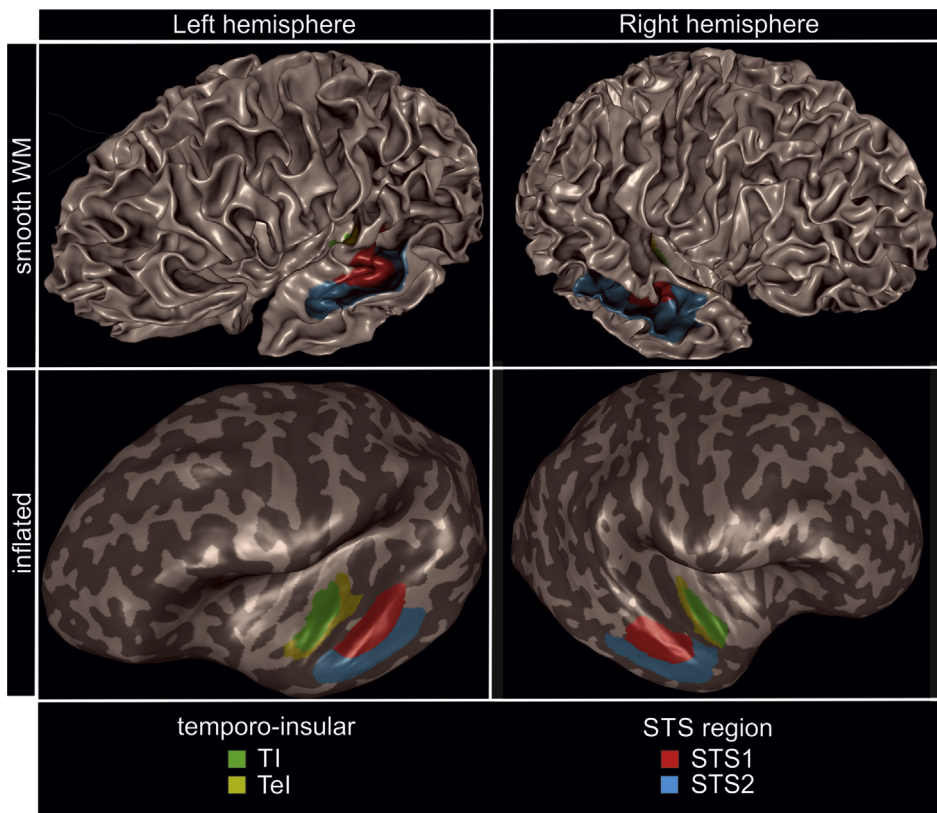


Fig. 11 – Areal surface on the BigBrain. The new areas were mapped in the BigBrain and their middle areal surface was depicted in smooth white matter (WM, top) and inflated mode (bottom).

cytoarchitectonic results the two areas run in parallel: TI is the medial area and Tel the lateral one. This is in line with a recent study of the human auditory cortex which found a medial and a lateral part of area PaI in the temporo-insular region (Fullerton & Pandya, 2007). The STS areas have no correspondence in these histochemical studies, as histochemically defined area STA seem to correspond to Te3.

4.2. Interpretation of STS areas in comparison to other maps

The STS came into focus of research, when functional imaging revealed its multimodal properties (Hein & Knight, 2008). Findings from neuroimaging revealed a functional segregation of the STS. For example, a functional imaging study compared spoken and written speech (Wilson, Bautista, McCarron, 2017). Spoken speech activated Heschl's gyrus up to the lateral surface of the STG (Te1-3 in this work), whereas the STS region was activated in both conditions. This response indicates linguistic processing for the STS region. The study proposed processing of lexical nodes associated with a region in the upper bank of the STS, and higher level taxonomic and syntactic processing for the lower bank. These functions correspond anatomically to areas STS1 and STS2 and are not well reflected in the classical maps. In Brodmann's map (1909), BA22 (Fig. 1) covers the convexity of the STG and would comprise both Te3 and STS1. The whole middle temporal gyrus was labeled as BA21 (Brodmann, 1909). Von Economo

and Koskinas (1925) largely followed Brodmann's division of the temporal lobe (see Table 1). The myeloarchitectonic study of Hopf (1954) showed that the STS region can be further subdivided. His myeloarchitectonic area profunda (Fig. 1C) is a long-stretched sulcal area that covers half of the dorsal bank of the sulcus and may correspond to area STS1. However, Hopf did not describe a further sulcal area, while the present study found a second area (i.e., STS2) on the lower bank of the sulcus. The existence of this area, however, is in agreement with findings of a tractography-based parcellation study of the MTG. A sulcal area was found on the lower bank of the STS reaching from the middle to the anterior part of the sulcus (Xu, Wang, Fan, Li, Zhang et al., 2015).

4.3. Extent of the areas in the BigBrain

The BigBrain (<http://bigbrain.loris.ca>) is a reference brain for microscopic data with a resolution of 20 μm isotropic. This high spatial resolution of the BigBrain was used to calculate and represent the areal surfaces. Reported areal surfaces refer to the middle areal surface. The middle areal thickness was also calculated and seems to be a good approximation for the cortical depth (Table 4). Von Economo and Koskinas (1925) provided cortical thicknesses in the range from 2.2 to 2.5 mm for area TA on the STG and 3.0–3.2 mm for area TE on the MTG. The values of the middle areal thickness increased from TI to Tel and are highest in the STS areas, but did not reach the values mentioned for the MTG. The extent of the

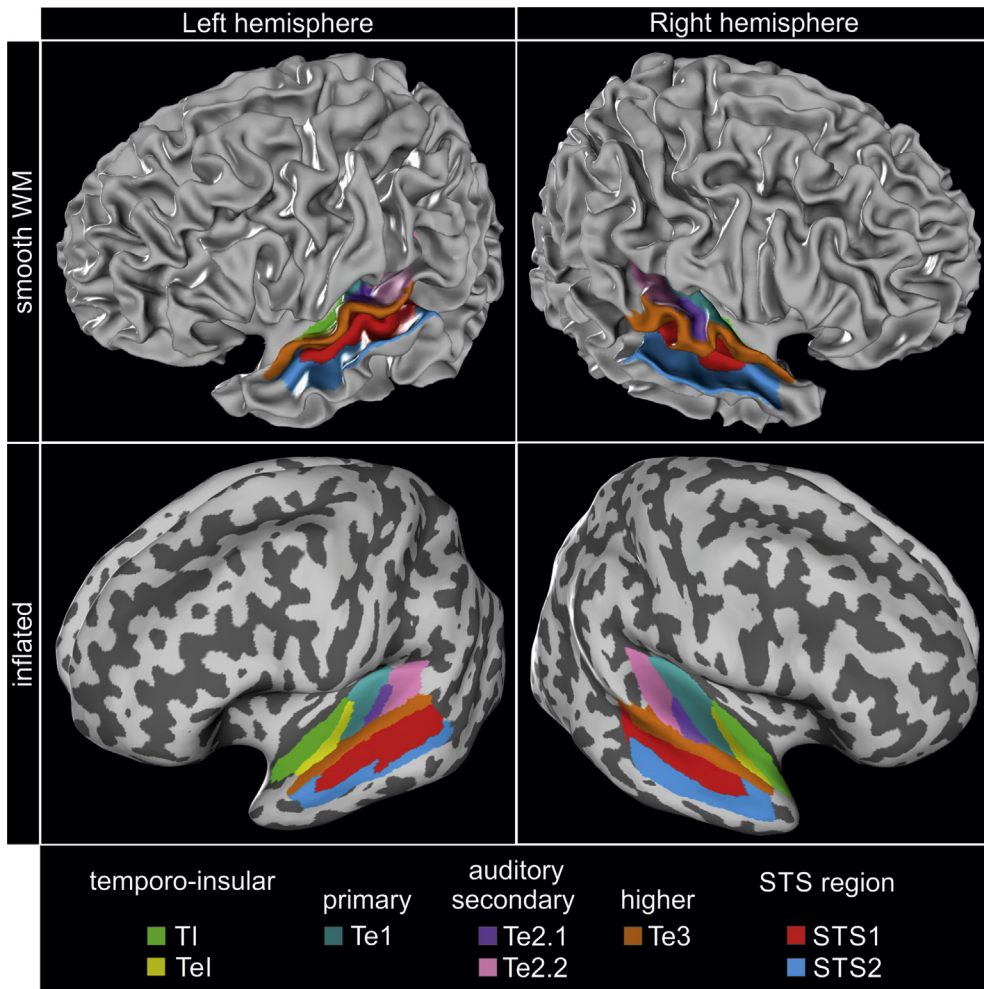


Fig. 12 – Maximum probability maps (mpms) of the STG. STG areas in the stereotaxic single-subject Colin 27 reference space. The maps were calculated on basis of the pmaps. Presentation in smooth white matter mode (top) and as inflated brains (bottom) to visualize the areas in the depths of the sulci.

areas relative to macroanatomical landmarks as Heschl's gyrus is the same as in the other brains. Also, the volumetric relations between the areas are comparable, even if the middle volumes of the areas are higher than the average areal volumes (Table 3). The difference of middle and the geometrical volumes are less than 4% and validated the reported method.

4.4. Lateralization of the new areas

Lateralization of language processing has been reported for Wernicke's region. With respect to sulcal patterns, it was found that the STS in the right hemisphere is deeper than in the left one (Leroy, Cai, Bogart, Dubois, Coulon et al., 2015), but no volumetric differences for the STS were reported (Ochiai, Grimault, Scavarda, Roch, Hori et al., 2004). This agrees with the present cytoarchitectonic study, which did not reveal left-right differences in areal volumes neither for the temporo-insular nor the STS areas. It also agrees with results from fMRI (functional magnetic resonance imaging) studies in

which both hemispheres were activated during speech processing, and lateralization was not found (Binder, Frost, Hammeke, Bellgowan, Springer et al., 2000; Obleser, Eisner, Kotz, 2008). The language areas were also analyzed in a resting-state study with respect to lateralization; this study found only a left lateralization for the posterior STS, but not for the middle and anterior part (McAvoy, Mitra, Coalson, d'Avossa, Keidel et al., 2016). The posterior STS was also found to be left-lateralized in a study investigating intelligible speech (Friederici, Kotz, Scott, Obleser, 2010). However, the coordinates of the peaks in MNI space ($y = -42$) of both studies are outside the localization of STS1 and STS2. Friederici et al. (2010) found that the anterior STS, which would correspond to our new areas, was activated bilaterally. Although the cytoarchitectonic study did not reveal any differences between the hemispheres, some areal functions seem to be lateralized. Our meta-analytic functional profiling found a left-hemispheric preference for drawing (STS1; TI), music comprehension (TI), covert reading, delay-discounting, and semantic discrimination (STS2) as well as dominance of the

Table 5 – Functional properties of the STG areas. Areas were activated by different paradigm classes according to the BrainMap taxonomy. Converging results of both forward and reverse inference are shown in colored boxes and are separately depicted for the left (LH) and right hemisphere (RH).

Paradigm class	TI		Tel		Te1		Te2.1		Te2.2		Te3		STS1		STS2	
	LH	RH	LH	RH	LH	RH	LH	RH	LH	RH	LH	RH	LH	RH	LH	RH
Pain Monitor/Discrimination		green														
Drawing	green															
Reading (Overt)			yellow													
Music Comprehension					teal											
Passive Listening							purple									
Tone Monitor/Discrimination																
Music Production																
Recitation/Repetition (Overt)			yellow				purple									
Pitch Monitor/Discrimination								purple								
Phonological Discrimination									pink							
Figurative Language										orange						
Semantic Monitor/Discrim.												red				
Theory of Mind																
Episodic Recall																
Imagined Object/Scenes																
Reading (Covert)																
Delay Discounting																

right hemisphere for pain discrimination (TI; [Supplementary Fig. S4](#)). These functional differences might not be necessarily reflected in volumetric differences between left- and right hemispheric areas.

4.5. Functional interpretation of the new areas

This study showed that TI and TeI, although neighboring areas, differ in their microstructure. TI has characteristics of the insular cortex, whereas TeI is similar to temporal areas. The discriminant analysis ([Fig. 9](#)) revealed that TeI is more closely related to area Te2.1. The MPM ([Fig. 12](#)) shows that primary area Te1 (petrol) is surrounded by secondary areas TeI and Te2.1. Te2 has a common border on the lateral surface of the gyrus with area Te3. This is in line with the core–belt–parabelt concept of macaques, where the primary auditory core region is surrounded by belt areas (probably our TeI medially and Te2.1 and Te2.2 laterally), and ends on the lateral surface in the parabelt region ([Pandya & Sanides, 1973](#); [Petkov, Kayser, Augath, Logothetis, 2006](#)). The core is connected to the belt areas, and the belt areas are connected with each other and the parabelt areas ([Clarke & Morosan, 2012](#)). The auditory areas in macaques were compared to human auditory areas in a study by [Fullerton and Pandya \(2007\)](#), which is a hint to possibly the same information processing in humans.

The human core to parabelt areas (Te1–3) are activated by all tasks requiring spectro-temporal analysis of sounds

([Table 5](#)), but the analysis for the temporo-insular region shows different functions for TI and TeI confirming our cytoarchitectonic results, in which TeI is more similar in its microstructure to Te2.1 than to its neighboring area TI. TI is activated by interoception (pain) and fine motor control (drawing), both insular-like functions. Music comprehension was found in both areas. The temporo-insular region is activated by sung speech, prosody and melody ([Brown, Martinez, Parsons, 2004](#); [Callan, Tsytsarev, Hanakawa, Callan, Katsuhara et al., 2006](#); [Jeffries, Fritz, Braun, 2003](#)). [Angulo-Perkins et al. \(2014\)](#) found that this region is only activated by music, not by speech. Another study has found abstract perception of speech on the Planum polare ([Hasson, Skipper, Nusbaum, Small, 2007](#)). The temporo-insular region was also activated by tasks involving melody and music ([Angulo-Perkins et al., 2014](#); [Barrett & Hall, 2006](#); [Brown et al., 2004](#); [Callan et al., 2006](#); [Koelsch, Gunter, von Cramon, Zysset, Lohmann et al., 2002](#); [Patterson, Uppenkamp, Johnsrude, Griffiths, 2002](#)), and prosody of language ([Friederici, Meyer, von Cramon, 2000](#); [Scott, Blank, Rosen, Wise, 2000](#)), which is supposed to be a major function of this region and which can be explained by the tone/pitch discrimination of the area TeI. These activations can be better described by the new maps of the temporo-insular region than by the macrolabels – anterior part of BA22 and the posterior part of BA38.

The same is true for the segregation of the STS cortex, where the functional profiling revealed different functional

roles for the upper and lower bank. Accordingly, STS1 is linked to figurative language, semantic discrimination and theory-of-mind cognition, whereas STS2 is linked to episodic recall, object/scene imagination, covert reading, and delay-discounting. In a study by Wilson (2017), the upper bank was activated by backward speech and may be processing phonological word forms, whereas the lower bank showed little to no response to backwards speech and is likely to perform a higher level of linguistic processing. This higher linguistic processing would require memory retrieval and imagination of object and scenes to connect the words to their meaning. Area STS2 was connected to precuneus, medial frontal pole and gyrus cinguli (Bludau et al., 2014; Xu et al., 2015), structures that are involved in working memory. It was also found that the mid-to-anterior part of the STS was activated by tasks requiring the processing of intelligible speech (Clos, Langner, Meyer, Oechslin, Zilles et al., 2014; Evans, Kyong, Rosen, Golestani, Warren et al., 2014; Kyong, Scott, Rosen, Howe, Agnew et al., 2014; Shultz, Vouloumanos, Pelpfrey, 2012) and voice (Belin, Zatorre, Lafaille, Ahad, Pike, 2000; Pernet, McAleer, Latinus, Gorgolewski, Charest et al., 2015; Schall, Kiebel, Maess, von Kriegstein, 2015). It seems that the spectro-temporal information of the auditory input is analyzed in the dorsal plane and the lateral free surface of the STG. This region largely corresponds to areas Te1-3. The newly described areas of the STS however, are cytoarchitectonically and functionally distinct from this auditory region. This notion is supported by functional profiling (see Table 5). Thus, our new maps seem to better reflect the activation differences found in functional neuroimaging studies than does the unitary representation of Brodmann's area BA22, which comprises Te3 and STS1.

For the structural/functional relationship of the areas, we used the BrainMap database with a resolution of $2 \times 2 \times 2 \text{ mm}^3$. Although this analysis provided sound results, the resolution of the BrainMap database does not match the precision of our maps due to technical constraints of fMRI. The functional properties of small areas, especially those of the temporo-insular region, would benefit from further investigations with ultra-high field fMRI. Thus, a more fine-grained functional parcellation of these areas would be possible in future, as it has been previously reported for the auditory (Moerel, De Martino, Kemper, Schmitter, Vu et al., 2018) and visual cortices (Kemper, De Martino, Emmerling, Yacoub, Goebel, 2018).

In conclusion, the present study delineates four new cytoarchitectonic areas, TI and TeI medial, and STS1 and STS2 lateral, of primary and early auditory cortex. A comprehensive map of the STG is provided. The areas of the temporo-insular region show a dichotomy in their microstructure: area TI is more insular-like, while area TeI has cytoarchitectonic characteristics of secondary auditory areas, which confirms the core-belt concept of macaques in the human brain. The STS areas are functionally and cytoarchitectonically different from the parabelt area Te3. Area Te3 is engaged in the spectro-temporal analysis of auditory input, whereas the STS areas are activated during higher language and cognitive tasks.

Data availability

Brain maps: <https://kg.ebrains.eu/search>.

Cytoarchitectonic data: <https://www.humanbrainproject.eu/en/explore-the-brain/>

The conditions of our ethics approval do not permit public archiving of anonymized study data. Readers seeking access to the data should contact the lead author Daniel Zachlod. Specifically, requestors must complete a formal data sharing agreement.

Legal copyright restrictions do not permit us to publicly archive the full set of data analysis and preprocessing code. Readers seeking access to this code are advised to contact the lead author Daniel Zachlod. Access to the code will be permitted as part of a collaboration upon a case-by-case decision. Owner of the code copyrights is the Forschungszentrum Jülich GmbH.

Funding

This project has received funding from the European Union's Horizon 2020 Research and Innovation Programme under Grant Agreement No. 785907 (HBP SGA2).

Ethical statement

The brains of ten subjects were obtained through the body donor program of the Department of anatomy at the University of Düsseldorf in accordance to the rules of the local ethics committee (# 4863).

Author contributions

DZ mapped the STS region, analyzed the results and wrote the manuscript, BR provided the maps of the temporo-insular cortex, SB performed the cluster analysis, HM calculated the maps in the reference space, RL performed the functional profiling, KZ co-developed the study design, KA developed the study, analyzed and interpreted the results. All authors read and critically revised the manuscript and approved its publication.

Declaration of Competing Interest

None declared.

Notes

We report how we determined our sample size, all data exclusions, all inclusion/exclusion criteria, whether inclusion/exclusion criteria were established prior to data analysis, all manipulations, and all measures in the study.

No part of the study procedures and study analysis was pre-registered prior to the research being conducted.

Acknowledgment

The authors would like to thank the laboratory team Markus Cremer, Sabrina Behuet and Jessica Teske-Bausch, Ferdag Kocaer and Ursula Blohm, for the preparation of histological tissue.

Supplementary data

Supplementary data to this article can be found online at <https://doi.org/10.1016/j.cortex.2020.02.021>.

REFERENCES

- Amunts, K., Armstrong, E., Malikovic, A., Hömke, L., Mohlberg, H., Schleicher, A., et al. (2007). Gender-specific left–right asymmetries in human visual cortex. *The Journal of Neuroscience*, 27(6), 1356–1364. <https://doi.org/10.1523/jneurosci.4753-06.2007>.
- Amunts, K., Kedo, O., Kindler, M., Pieperhoff, P., Mohlberg, H., Shah, N. J., et al. (2005). Cytoarchitectonic mapping of the human amygdala, hippocampal region and entorhinal cortex: Intersubject variability and probability maps. *Anatomy and Embryology*, 210(5–6), 343–352. <https://doi.org/10.1007/s00429-005-0025-5>.
- Amunts, K., Lepage, C., Borgeat, L., Mohlberg, H., Dickscheid, T., Rousseau, M.-É., et al. (2013). BigBrain: An ultrahigh-resolution 3D human brain model. *Science*, 340(6139), 1472–1475.
- Amunts, K., Schleicher, A., Burgel, U., Mohlberg, H., Uylings, H. B., & Zilles, K. (1999). Broca's region revisited: Cytoarchitecture and intersubject variability. *Journal of Comparative Neurology*, 412(2), 319–341.
- Amunts, K., Weiss, P. H., Mohlberg, H., Pieperhoff, P., Eickhoff, S., Gurd, J. M., et al. (2004). Analysis of neural mechanisms underlying verbal fluency in cytoarchitectonically defined stereotaxic space – The roles of Brodmann areas 44 and 45. *NeuroImage*, 22(1), 42–56. <https://doi.org/10.1016/j.neuroimage.2003.12.031>.
- Angulo-Perkins, A., Aube, W., Peretz, I., Barrios, F. A., Armony, J. L., & Concha, L. (2014). Music listening engages specific cortical regions within the temporal lobes: Differences between musicians and non-musicians. *Cortex*, 59, 126–137. <https://doi.org/10.1016/j.cortex.2014.07.013>.
- Barrett, D. J., & Hall, D. A. (2006). Response preferences for “what” and “where” in human non-primary auditory cortex. *NeuroImage*, 32(2), 968–977. <https://doi.org/10.1016/j.neuroimage.2006.03.050>.
- Belin, P., Zatorre, R. J., Lafaille, P., Ahad, P., & Pike, B. (2000). Voice-selective areas in human auditory cortex. *Nature*, 403(6767), 309–312. <https://doi.org/10.1038/35002078>.
- Binder, J. R. (2015). The Wernicke area: Modern evidence and a reinterpretation. *Neurology*, 85(24), 2170–2175. <https://doi.org/10.1212/WNL.0000000000002219>.
- Binder, J. R. (2017). Current controversies on Wernicke's area and its role in language. *Current Neurology and Neuroscience Reports*, 17(8), 58. <https://doi.org/10.1007/s11910-017-0764-8>.
- Binder, J. R., Frost, J. A., Hammeke, T. A., Bellgowan, P. S., Springer, J. A., Kaufman, J. N., et al. (2000). Human temporal lobe activation by speech and nonspeech sounds. *Cerebral Cortex*, 10(5), 512–528.
- Bludau, S., Eickhoff, S. B., Mohlberg, H., Caspers, S., Laird, A. R., Fox, P. T., et al. (2014). Cytoarchitecture, probability maps and functions of the human frontal pole. *NeuroImage*, 93(Pt 2), 260–275. <https://doi.org/10.1016/j.neuroimage.2013.05.052>.
- Bogen, J. E., & Bogen, G. (1976). Wernicke's region – where is it? *Annals of the New York Academy of Sciences*, 280(1), 834–843.
- Brodmann, K. (1909). *Vergleichende lokalisationslehre der Großhirnrinde*. Leipzig: Barth.
- Brown, S., Martinez, M. J., & Parsons, L. M. (2004). Passive music listening spontaneously engages limbic and paralimbic systems. *NeuroReport*, 15(13), 2033–2037.
- Callan, D. E., Tsytarev, V., Hanakawa, T., Callan, A. M., Katsuhara, M., Fukuyama, H., et al. (2006). Song and speech: Brain regions involved with perception and covert production. *NeuroImage*, 31(3), 1327–1342. <https://doi.org/10.1016/j.neuroimage.2006.01.036>.
- Clarke, S., & Morosan, P. (2012). Architecture, connectivity, and transmitter receptors of human auditory cortex. In D. Poeppel, T. Overath, A. N. Popper, & R. R. Fay (Eds.), *The human auditory cortex* (pp. 11–38). New York, NY: Springer New York.
- Clos, M., Langner, R., Meyer, M., Oechslin, M. S., Zilles, K., & Eickhoff, S. B. (2014). Effects of prior information on decoding degraded speech: An fMRI study. *Human Brain Mapping*, 35(1), 61–74.
- Collins, D. L., Neelin, P., Peters, T. M., & Evans, A. C. (1994). Automatic 3d intersubject registration of MR volumetric data in standardized Talairach space. *Journal of Computer Assisted Tomography*, 18(2), 192–205.
- Covington, M. A., He, C., Brown, C., Naçi, L., McClain, J. T., Fjordbak, B. S., et al. (2005). Schizophrenia and the structure of language: The linguist's view. *Schizophrenia Research*, 77(1), 85–98.
- DeWitt, I., & Rauschecker, J. P. (2012). Phoneme and word recognition in the auditory ventral stream. *Proceedings of the National Academy of Sciences*, 109(8), E505–E514. <https://doi.org/10.1073/pnas.1113427109>.
- Diederen, K. M., Daalman, K., de Weijer, A. D., Neggers, S. F., van Gastel, W., Blom, J. D., et al. (2012). Auditory hallucinations elicit similar brain activation in psychotic and nonpsychotic individuals. *Schizophrenia Bulletin*, 38(5), 1074–1082. <https://doi.org/10.1093/schbul/sbr033>.
- Eickhoff, S. B., Bzdok, D., Laird, A. R., Roski, C., Caspers, S., Zilles, K., et al. (2011). Co-activation patterns distinguish cortical modules, their connectivity and functional differentiation. *NeuroImage*, 57(3), 938–949.
- Eickhoff, S. B., Paus, T., Caspers, S., Grosbras, M. H., Evans, A. C., Zilles, K., et al. (2007). Assignment of functional activations to probabilistic cytoarchitectonic areas revisited. *NeuroImage*, 36(3), 511–521. <https://doi.org/10.1016/j.neuroimage.2007.03.060>.
- Eickhoff, S. B., Stephan, K. E., Mohlberg, H., Grefkes, C., Fink, G. R., Amunts, K., et al. (2005). A new SPM toolbox for combining probabilistic cytoarchitectonic maps and functional imaging data. *NeuroImage*, 25(4), 1325–1335. <https://doi.org/10.1016/j.neuroimage.2004.12.034>.
- Eigsti, I.-M., de Marchena, A. B., Schuh, J. M., & Kelley, E. (2011). Language acquisition in autism spectrum disorders: A developmental review. *Research in Autism Spectrum Disorders*, 5(2), 681–691.
- Evans, A. C., Collins, D. L., Mills, S. R., Brown, E. D., Kelly, R. L., & Peters, T. M. (1993). 3d statistical neuroanatomical models from 305 MRI volumes. *Nuclear Science Symposium & Medical Imaging Conference*, 1–3, 1813–1817.
- Evans, S., Kyong, J. S., Rosen, S., Golestani, N., Warren, J. E., McGettigan, C., et al. (2014). The pathways for intelligible speech: Multivariate and univariate perspectives. *Cerebral Cortex*, 24(9), 2350–2361. <https://doi.org/10.1093/cercor/bht083>.
- Fox, P. T., Laird, A. R., Fox, S. P., Fox, P. M., Uecker, A. M., Crank, M., et al. (2005). BrainMap taxonomy of experimental

- design: Description and evaluation. *Human Brain Mapping*, 25(1), 185–198.
- Friederici, A. D. (2012). The cortical language circuit: From auditory perception to sentence comprehension. *Trends in Cognitive Sciences*, 16(5), 262–268.
- Friederici, A. D., Kotz, S. A., Scott, S. K., & Obleser, J. (2010). Disentangling syntax and intelligibility in auditory language comprehension. *Human Brain Mapping*, 31(3), 448–457. <https://doi.org/10.1002/hbm.20878>.
- Friederici, A. D., Meyer, M., & von Cramon, D. Y. (2000). Auditory language comprehension: An event-related fMRI study on the processing of syntactic and lexical information. *Brain and Language*, 74(2), 289–300. <https://doi.org/10.1006;brln.2000.2313>.
- Fullerton, B. C., & Pandya, D. N. (2007). Architectonic analysis of the auditory-related areas of the superior temporal region in human brain. *Journal of Comparative Neurology*, 504(5), 470–498.
- Galaburda, A., & Sanides, F. (1980). Cytoarchitectonic organization of the human auditory cortex. *Journal of Comparative Neurology*, 190(3), 597–610. <https://doi.org/10.1002/cne.901900312>.
- Gendry Meresse, I., Zilbovicius, M., Boddaert, N., Robel, L., Philippe, A., Sfaello, I., et al. (2005). Autism severity and temporal lobe functional abnormalities. *Annals of Neurology*, 58(3), 466–469.
- Hasson, U., Skipper, J. I., Nusbaum, H. C., & Small, S. L. (2007). Abstract coding of audiovisual speech: Beyond sensory representation. *Neuron*, 56(6), 1116–1126. <https://doi.org/10.1016/j.neuron.2007.09.037>.
- Hein, G., & Knight, R. T. (2008). Superior temporal sulcus – It's my area: Or is it? *Journal of Cognitive Neuroscience*, 20(12), 2125–2136. <https://doi.org/10.1162/jocn.2008.20148>.
- Holmes, C. J., Hoge, R., Collins, L., Woods, R., Toga, A. W., & Evans, A. C. (1998). Enhancement of MR images using registration for signal averaging. *Journal of Computer Assisted Tomography*, 22(2), 324–333.
- Hörmke, L. (2006). A multigrid method for anisotropic PDEs in elastic image registration. *Numerical Linear Algebra with Applications*, 13(2–3), 215–229. <https://doi.org/10.1002/nla.477>.
- Hopf, A. (1954). Die Myeloarchitektonik des Isocortex temporalis beim Menschen. *Journal für Hirnforschung*, 1, 208–279.
- Jeffries, K., Fritz, J. B., & Braun, A. R. (2003). Words in melody: An H215O PET study of brain activation during singing and speaking. *NeuroReport*, 14(5), 749–754.
- Kemper, V. G., De Martino, F., Emmerling, T. C., Yacoub, E., & Goebel, R. (2018). High resolution data analysis strategies for mesoscale human functional MRI at 7 and 9.4 T. *NeuroImage*, 164, 48–58.
- Koelsch, S., Gunter, T. C., von Cramon, D. Y., Zysset, S., Lohmann, G., & Friederici, A. D. (2002). Bach speaks: A cortical “language-network” serves the processing of music. *NeuroImage*, 17(2), 956–966.
- Kretschmann, H. (1971). Biometric studies on the fresh volume of human brain regions. *Verhandlungen der Anatomischen Gesellschaft*, 65, 139.
- Kurth, F., Eickhoff, S. B., Schleicher, A., Hoemke, L., Zilles, K., & Amunts, K. (2010). Cytoarchitecture and probabilistic maps of the human posterior insular cortex. *Cerebral Cortex*, 20(6), 1448–1461. <https://doi.org/10.1093/cercor/bhp208>.
- Kyong, J. S., Scott, S. K., Rosen, S., Howe, T. B., Agnew, Z. K., & McGettigan, C. (2014). Exploring the roles of spectral detail and intonation contour in speech intelligibility: An fMRI study. *Journal of Cognitive Neuroscience*, 26(8), 1748–1763. https://doi.org/10.1162/jocn_a_00583.
- Laird, A. R., Eickhoff, S. B., Kurth, F., Fox, P. M., Uecker, A. M., Turner, J. A., et al. (2009). ALE meta-analysis workflows via the brainmap database: Progress towards a probabilistic functional brain atlas. *Frontiers in Neuroinformatics*, 3, 23.
- Langner, R., Gieslik, E. C., Behrwald, S. D., Roski, C., Caspers, S., Amunts, K., et al. (2015). Aging and response conflict solution: Behavioural and functional connectivity changes. *Brain Structure and Function*, 220(3), 1739–1757.
- Leroy, F., Cai, Q., Bogart, S. L., Dubois, J., Coulon, O., Monzalvo, K., et al. (2015). New human-specific brain landmark: The depth asymmetry of superior temporal sulcus. *Proceedings of the National Academy of Sciences of the United States of America*, 112(4), 1208–1213. <https://doi.org/10.1073/pnas.1412389112>.
- Lichtheim, L. (1884). Die verschiedenen Symptomenbilder der Aphasie. *Archiv für Psychiatrie und Nervenkrankheiten*, 15, 822–828.
- Mahalanobis, P. C., Majumdar, D., Yeatts, M., & Rao, C. R. (1949). Anthropometric survey of the United Provinces, 1941: A statistical study. *Sankhyā: The Indian Journal of Statistics*, 89–324.
- Matsumoto, H., Simmons, A., Williams, S., Hadjulis, M., Pipe, R., Murray, R., et al. (2001). Superior temporal gyrus abnormalities in early-onset schizophrenia: Similarities and differences with adult-onset schizophrenia. *American Journal of Psychiatry*, 158(8), 1299–1304.
- McAvoy, M., Mitra, A., Coalson, R. S., d'Avossa, G., Keidel, J. L., Petersen, S. E., et al. (2016). Unmasking language lateralization in human brain intrinsic activity. *Cerebral Cortex*, 26(4), 1733–1746. <https://doi.org/10.1093/cercor/bhv007>.
- Merker, B. (1983). Silver staining of cell bodies by means of physical development. *Journal of Neuroscience Methods*, 9(3), 235–241.
- Mesulam, M. M., Rogalski, E. J., Wieneke, C., Hurley, R. S., Geula, C., Bigio, E. H., et al. (2014). Primary progressive aphasia and the evolving neurology of the language network. *Nature Reviews Neurology*, 10(10), 554–569. <https://doi.org/10.1038/nrneurol.2014.159>.
- Moerel, M., De Martino, F., & Formisano, E. (2014). An anatomical and functional topography of human auditory cortical areas. *Frontiers in Neuroscience*, 8, 225.
- Moerel, M., De Martino, F., Kemper, V. G., Schmitter, S., Vu, A. T., Ügürbil, K., et al. (2018). Sensitivity and specificity considerations for fMRI encoding, decoding, and mapping of auditory cortex at ultra-high field. *NeuroImage*, 164, 18–31.
- Morosan, P., Rademacher, J., Palomero-Gallagher, N., & Zilles, K. (2005a). Anatomical organization of the human auditory cortex: Cytoarchitecture and transmitter receptors. New York: Psychology Press.
- Morosan, P., Rademacher, J., Schleicher, A., Amunts, K., Schormann, T., & Zilles, K. (2001). Human primary auditory cortex: Cytoarchitectonic subdivisions and mapping into a spatial reference system. *NeuroImage*, 13(4), 684–701. <https://doi.org/10.1006/nimg.2000.0715>.
- Morosan, P., Schleicher, A., Amunts, K., & Zilles, K. (2005b). Multimodal architectonic mapping of human superior temporal gyrus. *Anatomy and Embryology*, 210(5–6), 401–406. <https://doi.org/10.1007/s00429-005-0029-1>.
- Obleser, J., Eisner, F., & Kotz, S. A. (2008). Bilateral speech comprehension reflects differential sensitivity to spectral and temporal features. *The Journal of Neuroscience*, 28(32), 8116–8123. <https://doi.org/10.1523/JNEUROSCI.1290-08.2008>.
- Ochiai, T., Grimalt, S., Scavarda, D., Roch, G., Hori, T., Riviere, D., et al. (2004). Sulcal pattern and morphology of the superior temporal sulcus. *NeuroImage*, 22(2), 706–719. <https://doi.org/10.1016/j.neuroimage.2004.01.023>.
- Pandya, D. N., & Sanides, F. (1973). Architectonic parcellation of the temporal operculum in rhesus monkey and its projection pattern. *Zeitschrift für Anatomie und Entwicklungsgeschichte*, 139(2), 127–161.
- Patterson, R. D., Uppenkamp, S., Johnsrude, I. S., & Griffiths, T. D. (2002). The processing of temporal pitch and melody information in auditory cortex. *Neuron*, 36(4), 767–776.

- Pernet, C. R., McAleer, P., Latinus, M., Gorgolewski, K. J., Charest, I., Bestelmeyer, P. E., et al. (2015). The human voice areas: Spatial organization and inter-individual variability in temporal and extra-temporal cortices. *NeuroImage*, 119, 164–174. <https://doi.org/10.1016/j.neuroimage.2015.06.050>.
- Petkov, C. I., Kayser, C., Augath, M., & Logothetis, N. K. (2006). Functional imaging reveals numerous fields in the monkey auditory cortex. *PLoS Biology*, 4(7), e215.
- Rivier, F., & Clarke, S. (1997). Cytochrome oxidase, acetylcholinesterase, and NADPH-diaphorase staining in human supratemporal and insular cortex: Evidence for multiple auditory areas. *NeuroImage*, 6(4), 288–304.
- Schall, S., Kiebel, S. J., Maess, B., & von Kriegstein, K. (2015). Voice identity recognition: Functional division of the right STS and its behavioral relevance. *Journal of Cognitive Neuroscience*, 27(2), 280–291. https://doi.org/10.1162/jocn_a_00707.
- Schleicher, A., Morosan, P., Amunts, K., & Zilles, K. (2009). Quantitative architectural analysis: A new approach to cortical mapping. *Journal of Autism and Developmental Disorders*, 39(11), 1568–1581. <https://doi.org/10.1007/s10803-009-0790-8>.
- Schleicher, A., Palomero-Gallagher, N., Morosan, P., Eickhoff, S. B., Kowalski, T., de Vos, K., et al. (2005). Quantitative architectural analysis: A new approach to cortical mapping. *Anatomy and Embryology*, 210(5–6), 373–386. <https://doi.org/10.1007/s00429-005-0028-2>.
- Scott, S. K., Blank, C. C., Rosen, S., & Wise, R. J. (2000). Identification of a pathway for intelligible speech in the left temporal lobe. *Brain*, 123 Pt 12, 2400–2406.
- Shultz, S., Vouloumanos, A., & Pelpfrey, K. (2012). The superior temporal sulcus differentiates communicative and noncommunicative auditory signals. *Journal of Cognitive Neuroscience*, 24(5), 1224–1232. https://doi.org/10.1162/jocn_a_00208.
- von Economo, C., & Horn, L. (1930b). Über Windungsrelief, Maße und Rindenarchitektonik der Supratemporalfläche, ihre individuellen und ihre Seitenunterschiede. *Zeitschrift für die gesamte Neurologie und Psychiatrie*, 130(1), 678–757.
- Von Economo, C., & Koskinas, G. (1925). Die Cytoarchitektur der Hirnrinde des erwachsenen Menschen. Berlin: Springer.
- Wagstyl, K., Lepage, C., Bludau, S., Zilles, K., Fletcher, P. C., Amunts, K., et al. (2018). Mapping cortical laminar structure in the 3d bigbrain. *Cerebral Cortex*, 28(7), 2551–2562.
- Wallace, M. N., Johnston, P. W., & Palmer, A. R. (2002). Histochemical identification of cortical areas in the auditory region of the human brain. *Experimental Brain Research*, 143(4), 499–508.
- Ward, J. H. (1963). Hierarchical grouping to optimize an objective function. *Journal of the American Statistical Association*, 58(301), 236. <https://doi.org/10.2307/2282967>.
- Wernicke, C. (1874). *Der aphasische symptomencomplex: Eine psychologische studie auf anatomischer basis*. Cohn.
- Wilson, S. M., Bautista, A., & McCarron, A. (2017). Convergence of spoken and written language processing in the superior temporal sulcus. *NeuroImage*, 171, 62–74. <https://doi.org/10.1016/j.neuroimage.2017.12.068>.
- Wree, A., Schleicher, A., & Zilles, K. (1982). Estimation of volume fractions in nervous tissue with an image analyzer. *Journal of Neuroscience Methods*, 6(1–2), 29–43.
- Xu, J., Wang, J., Fan, L., Li, H., Zhang, W., Hu, Q., et al. (2015). Tractography-based parcellation of the human middle temporal gyrus. *Scientific Reports*, 5, 18883. <https://doi.org/10.1038/srep18883>.